

# Galactic inflow and wind recycling rates in the EAGLE simulations

Peter D. Mitchell<sup>\*1</sup>, Joop Schaye<sup>1</sup> and Richard G. Bower<sup>2</sup>

<sup>1</sup>*Leiden Observatory, Leiden University, P.O. Box 9513, 2300 RA Leiden, the Netherlands*

<sup>2</sup>*Institute for Computational Cosmology, Department of Physics, Durham University, South Road, Durham, DH1 3LE, UK*

10 August 2020

## ABSTRACT

The role of galactic wind recycling represents one of the largest unknowns in galaxy evolution, as any contribution of recycling to galaxy growth is largely degenerate with the inflow rates of first-time infalling material, and the rates with which outflowing gas and metals are driven from galaxies. We present measurements of the efficiency of wind recycling from the EAGLE cosmological simulation project, leveraging the statistical power of large-volume simulations that reproduce a realistic galaxy population. We study wind recycling at the halo scale, i.e. gas that has been ejected beyond the halo virial radius, and at the galaxy scale, i.e. gas that has been ejected from the ISM to at least  $\approx 10\%$  of the virial radius (thus excluding smaller-scale galactic fountains). Galaxy-scale wind recycling is generally inefficient, with a characteristic return timescale that is comparable or longer than a Hubble time, and with an efficiency that clearly peaks at the characteristic halo mass of  $M_{200} = 10^{12} M_{\odot}$ . Correspondingly, the majority of gas being accreted onto galaxies in EAGLE is infalling for the first time. Recycling is more efficient at the halo scale, with values that differ by orders of magnitude from those assumed by semi-analytic galaxy formation models. Differences in the efficiency of wind recycling with other hydrodynamical simulations are currently difficult to assess, but are likely smaller. We are able to show that the fractional contribution of wind recycling to galaxy growth is smaller in EAGLE than in some other simulations. In addition to measurements of wind recycling, we study the efficiency with which first-time infalling material is accreted through the virial radius, and also the efficiency with which this material reaches the ISM. We find that cumulative first-time gas accretion rates at the virial radius are reduced relative to the expectation from dark matter accretion for haloes with mass,  $M_{200} < 10^{12} M_{\odot}$ , indicating efficient preventative feedback on halo scales.

**Key words:** galaxies: formation – galaxies: evolution – galaxies: haloes – galaxies: stellar content

## 1 INTRODUCTION

In the modern cosmological paradigm, galaxies are thought to form within dark matter haloes, which represent collapsed density fluctuations that grew from a near-uniform density field via gravitational instability. Dark matter haloes grow gradually by the accretion of smaller haloes, and baryonic accretion onto haloes is expected to trace this process, with half of the current stellar mass density of the Universe having formed after  $z \approx 1.3$  (Madau & Dickinson 2014). In this picture, actively star-forming galaxies continually accrete gas from their wider environments, and this in turn helps to explain the observed chemical abundances of stars (e.g. Larson 1972), and the relatively short inferred gas depletion timescales of star-forming galaxies (e.g. Scoville et al. 2017).

While there is strong theoretical and indirect observational evidence for sustained gas accretion onto the interstellar medium (ISM) of galaxies, direct measurements of gaseous inflow rates have remained inaccessible, owing primarily to the tenuous low-density nature of extra-galactic gas, and to the weak expected kinematic signature (relative for example to the very strong kinematic signature of feedback-driven galactic outflows). Various observations that trace inflowing gas have been reported however, both for the Milky Way and for extra-galactic sources (e.g. Rubin et al. 2012; Fox et al. 2014; Turner et al. 2017; Bish et al. 2019; Roberts-Borsani & Saintonge 2019; Zabl et al. 2019).

With a paucity of strong observational constraints, cosmological simulations have been used extensively as an alternative way to study gas accretion onto haloes and galaxies (e.g. Kereš et al. 2005; Faucher-Giguère et al. 2011; van de Voort et al. 2011; Nelson et al. 2013; Romano-Díaz et al. 2017; van de Voort et al. 2017; Correa

\* E-mail: mitchell@strw.leidenuniv.nl

et al. 2018ba). Simulations have predicted, for example, the presence of filamentary accretion streams, reflecting the larger scale filamentary structure of the cosmic web (e.g. Katz et al. 2003; Dekel & Birnboim 2006). Simulation predictions for inflows are expected to be strongly model dependent however, since it has been demonstrated that feedback processes (the implementation of which remains highly uncertain in simulations) modulate gaseous inflow rates, either by reducing the rate of first-time gaseous infall (e.g. Nelson et al. 2015), or by the recycling of previously ejected wind material (e.g. Oppenheimer et al. 2010).

The spatial and halo mass scales for which these processes play a significant role have been studied in a variety of simulations. Broadly speaking, feedback processes are expected to strongly modulate the accretion rates of gas onto the ISM of galaxies (e.g. Oppenheimer et al. 2010; Faucher-Giguère et al. 2011; van de Voort et al. 2011; Nelson et al. 2015; Anglés-Alcázar et al. 2017; Correa et al. 2018a), and to shape the content of the circum-galactic medium (e.g. Hafen et al. 2019). The effect of feedback processes on inflows at the scale of the halo virial radius is less clear, although effects are often reported for haloes with masses  $M_{200} < 10^{12} M_{\odot}$  (van de Voort et al. 2011; Faucher-Giguère et al. 2011; Christensen et al. 2016; Tollet et al. 2019). The role of wind recycling is also debated, with studies reporting that between 50% (Übler et al. 2014) and 90% (Grand et al. 2019) of gaseous inflow onto galaxies is recycled for different cosmological simulations (see van de Voort 2017 for a recent review). Furthermore, recent studies have highlighted the potential importance of the transfer of gas between galaxies (Anglés-Alcázar et al. 2017), and haloes (Borrow et al. 2020), due to feedback related processes.

The potential role of wind recycling has also been explored in more idealised analytic and semi-analytical models of galaxy formation. In particular, authors have highlighted how a strong dependence of the efficiency of wind recycling with halo mass can help reconcile models with the observed evolution of the galaxy stellar mass function (Henriques et al. 2013; Hirschmann et al. 2016), and that a strongly time-evolving recycling efficiency can explain the observed evolution of galaxy specific star formation rates (Mitchell et al. 2014), which is generally not reproduced in models and simulations (e.g. Daddi et al. 2007; Mitchell et al. 2014; Kaviraj et al. 2017; Pillepich et al. 2018). Generally speaking, these studies demonstrate that gas recycling (if it proceeds over timescales that are comparable or longer than the other timescales that govern galaxy growth, and with strong mass and/or redshift dependence) is a highly promising mechanism for decoupling the growth of galaxies from the growth of their host dark matter haloes, which is required to explain various observational trends.

Recent years have seen the development of cosmological simulations that produce a relatively realistic population of galaxies when compared to current observational constraints, and that simulate the galaxy population over a representative volume (e.g. Vogelsberger et al. 2014; Schaye et al. 2015). The statistical sample sizes afforded by such simulations greatly facilitate the study of correlations between gaseous inflows and other galaxy properties (such as radial metallicity gradients, Collacchioni et al. 2019), and to study the role of environment on accretion (van de Voort et al. 2017). The realism of these simulations affords additional confidence to the results, in contrast to the older simulations that did not reproduce the observed galaxy stellar mass function. As an example, Oppenheimer et al. (2010) find that wind recycling dominates gas accretion onto massive galaxies, but their simulations do not include AGN feedback, and so greatly over-predict the abundance of massive galaxies.

As one of the current state-of-the-art modern large-volume cosmological simulations, the EAGLE simulation project simulates the formation and evolution of galaxies within the  $\Lambda$  Cold Dark Matter model, integrating periodic cubic boxes (up to  $100^3 \text{ Mpc}^3$  in volume) down to  $z = 0$  (Schaye et al. 2015; Crain et al. 2015). With a fiducial baryonic particle mass of  $1.81 \times 10^6 M_{\odot}$ , EAGLE resolves galaxies (with at least 100 stellar particles) over roughly five orders of magnitude in halo mass ( $10^{11} < M_{200} < 10^{14}$ ). EAGLE has been used to study gas accretion onto haloes and galaxies, with individual studies focussing on the dichotomy between cold and hot accretion (Correa et al. 2018b), the impact of changing feedback models on gas accretion (Correa et al. 2018a), the impact of environment (van de Voort et al. 2017), the angular momentum content of cooling coronal gas (Stevens et al. 2017), and the connection between accretion and radial metallicity gradients in galaxies (Collacchioni et al. 2019).

In this study, we extend these analyses by using EAGLE to explicitly track the gas that is ejected from galaxies and haloes, which enables quantitative measurements of the efficiency and role of recycled accretion, as well as the study of gas that is transferred between independent galaxies and haloes. This study also follows from Mitchell et al. (2020), in which we present measurements of outflows on galaxy and halo scales. In future work, we then intend to combine these measurements together, in order to explicitly study how the mass and redshift scalings for first-time inflows, outflows, and wind recycling act in conjunction to explain the origin and evolution of the scaling relations between galaxy stellar mass and halo mass, and between galaxy star formation rate and stellar mass.

Relative to other studies of inflows and recycling in cosmological simulations (e.g. Anglés-Alcázar et al. 2017; Grand et al. 2019), we take care to measure quantities that can be robustly mapped onto a simplified description of galaxy formation as a network of ordinary differential equations. Most pertinently, we track the evolution of gas that is accreted onto galaxies or haloes at any time during their evolution, rather than only the subset of stars and gas that is located within a galaxy at some final redshift of selection. This means we can assess the characteristic timescale for all ejected gas to return, rather than for only the subset of gas that has returned by a given redshift. We also attempt to (as far as is reasonably possible) present a robust comparison of how wind recycling proceeds between various recent simulations and models from the literature, and in doing so identify areas of consensus (or tension) in the current theoretical picture.

The layout of this study is as follows: we present details of the EAGLE simulations and our methodology in Section 2, we present our main results in Section 3, a comparison with other recent theoretical studies from the literature is presented in Section 4, and we summarise our results and conclusions in Section 5.

## 2 METHODS

### 2.1 Simulations and subgrid physics

We utilise the EAGLE suite of cosmological hydrodynamical simulations (Schaye et al. 2015), which have been publicly released (McAlpine et al. 2016). EAGLE simulates cubic periodic boxes of representative volumes with full gravity and smoothed particle hydrodynamics (SPH) using a modified version of the GADGET-3 code (last described in Springel 2005), and employs uniform resolution throughout each simulation. A  $\Lambda$ CDM cosmological model

is assumed, with parameters set following Planck Collaboration et al. (2014). “Subgrid” physics are implemented to account for relevant physical processes that are not resolved (e.g. star formation), and radiative cooling and heating are modelled assuming a uniform ultraviolet radiation background, assuming the gas to be optically thin and in ionization equilibrium. Ionization modelling is performed for 11 elements.

The simulation suite includes a *Reference* set of parameters for the subgrid physics model, calibrated at a fiducial numerical resolution to reproduce the following observational diagnostics of the  $z \approx 0$  galaxy population: the galaxy stellar mass function, the relationship between galaxy size and stellar mass, and the relationship between supermassive black hole (SMBH) mass and galaxy stellar mass. The largest EAGLE simulation simulates a  $(100 \text{ Mpc})^3$  volume with  $2 \times 1504^3$  particles, with a fiducial particle mass of  $1.8 \times 10^6 M_\odot$  for gas and  $9.7 \times 10^6 M_\odot$  for dark matter. Unless otherwise stated, all of the EAGLE measurements presented in this article are taken from this simulation. The suite also contains simulations run with variations of the Reference model parameters, including a simulation named *Recal*, for which the model parameters were (re)calibrated against the same observational constraints, but at eight times higher numerical mass resolution than that of the Reference model.

Star particles are allowed to form from gas particles that first pass the metallicity-dependent density threshold for the transition from the warm, atomic to the cold, molecular ISM, as derived by Schaye (2004):

$$n_{\text{H}}^* = \min \left( 0.1 \left( \frac{Z}{0.002} \right)^{-0.64}, 10 \right) \text{ cm}^{-3}, \quad (1)$$

where  $Z$  is the gas metallicity. In addition, star formation is restricted to gas particles with temperature within 0.5 dex from a temperature floor,  $T_{\text{eos}}$ , which corresponds to an imposed equation of state  $P_{\text{eos}} \propto \rho^{4/3}$ , normalised to a temperature of  $T = 8 \times 10^3 \text{ K}$  at a hydrogen number density of  $0.1 \text{ cm}^{-3}$  (Schaye & Dalla Vecchia 2008). Gas particles are artificially pressurised up to this floor, such that in practice the ISM of galaxies is stabilised in a warm phase, preventing radiative cooling from leading to runaway fragmentation on Jeans scales that are unresolved in the simulation.

Eligible gas particles are turned into stars stochastically, with the average rate given by

$$\psi = m_{\text{gas}} A (1 \text{ Mpc}^{-2})^{-n} \left( \frac{\gamma}{G} f_{\text{g}} P \right)^{(n-1)/2}, \quad (2)$$

where  $P$  is the local gas pressure,  $m_{\text{gas}}$  is the gas particle mass,  $\gamma = 5/3$  is the ratio of specific heats,  $G$  is the gravitational constant,  $f_{\text{g}}$  is the gas mass fraction (set to unity). As described in Schaye & Dalla Vecchia (2008), this corresponds to a Kennicutt-Schmidt law for a gas disk in vertical hydrostatic equilibrium, with the dependent variable transformed from gas surface density to pressure. Following observational constraints on the observed Kennicutt-Schmidt law,  $A$  and  $n$  are set to  $A = 1.515 \times 10^{-4} \text{ Mpc yr}^{-1} \text{ kpc}^{-2}$  and  $n = 1.4$  (Kennicutt 1998).

A simple stellar feedback model is implemented in EAGLE that conceptually accounts for the combined effects of energy injected into the ISM by radiation and stellar winds from young stars, as well as supernova explosions. Thermal energy is injected stochastically by a fixed temperature difference of  $\Delta T = 10^{7.5} \text{ K}$ , with a high value above the peak of the radiative cooling curve chosen to mitigate the effects of spurious radiative losses that are expected

to occur if the injected energy were to instead be spread more uniformly in a poorly resolved artificially pressurised warm medium (Dalla Vecchia & Schaye 2012). No kinetic energy or momentum is injected directly by the subgrid model. Stellar feedback energy is injected when stars reach an age of 30 Myr, at a rate set such that the average energy injected is  $f_{\text{th}} \times 8.73 \times 10^{15} \text{ erg g}^{-1}$  of stellar mass formed, where  $f_{\text{th}}$  is a model parameter. For  $f_{\text{th}} = 1$ , the expectation value for the number of feedback events per particle is of order unity, and the injected energy per unit stellar mass corresponds to that of a simple stellar population with a Chabrier initial mass function, assuming that  $6 - 100 M_\odot$  stars explode as supernovae, and that each supernova injects  $10^{51} \text{ erg}$  of energy.

In practice, it was found that while adopting  $f_{\text{th}} = 1$  reproduced the observed galaxy stellar mass function reasonably well, it was necessary to inject extra energy at the high densities for which numerical overcooling is expected in order to also reproduce the observed galaxy size-stellar mass relation (Schaye et al. 2015; Crain et al. 2015). The following form was adopted

$$f_{\text{th}} = f_{\text{th,min}} + \frac{f_{\text{th,max}} - f_{\text{th,min}}}{1 + \left( \frac{Z}{0.1Z_\odot} \right)^{n_Z} \left( \frac{n_{\text{H,birth}}}{n_{\text{H,0}}} \right)^{-n_n}}, \quad (3)$$

where  $f_{\text{th,min}}$  and  $f_{\text{th,max}}$  are model parameters that are the asymptotic values of a sigmoid function in metallicity, with a transition scale at a characteristic metallicity,  $0.1Z_\odot$  (above which radiative losses are expected to increase due to metal cooling, Wiersma et al. 2009), and with a width controlled by  $n_Z$ . The two asymptotes,  $f_{\text{th,min}}$  and  $f_{\text{th,max}}$ , are set to 0.3 and 3 respectively, such that between 0.3 and 3 times the canonical supernova energy is injected. The dependence on local gas density is controlled by model parameters,  $n_{\text{H,0}}$ , and  $n_n$ . For the Reference model,  $n_Z$  and  $n_n$  are both set to  $2/\ln(10)$ , and  $n_{\text{H,0}}$  is set to  $1.46 \text{ cm}^{-3}$ .<sup>1</sup>

Supermassive black hole (SMBH) seeds are inserted into haloes with mass  $> 10^{10} M_\odot/h$ , as identified on the fly by a friend-of-friends (FoF) algorithm, using a linking length set equal to 0.2 times the average inter-particle separation. SMBH particles then grow by merging with other black holes, or by accreting gas particles at a rate given by a version of the Bondi accretion, modified such that accretion is reduced if the surrounding gas is rotating rapidly relative to the local sound speed (Rosas-Guevara et al. 2015; Schaye et al. 2015).

Similar to stellar feedback, feedback from accreting SMBH particles is implemented by stochastically heating neighbouring gas particles by a fixed temperature jump (Booth & Schaye 2009), in this case set to  $10^{8.5} \text{ K}$  for the Reference model. Energy is injected on average at a rate given by

$$\dot{E}_{\text{AGN}} = \epsilon_{\text{f}} \epsilon_{\text{r}} \dot{m}_{\text{acc}} c^2, \quad (4)$$

where  $\dot{m}_{\text{acc}}$  is the gas mass accretion rate onto the SMBH,  $c$  is the speed of light,  $\epsilon_{\text{f}}$  is the fraction of the accreted rest mass energy which is radiated (set to 0.1), and  $\epsilon_{\text{r}}$  is a model parameter which sets the fraction of the radiated energy that couples to the ISM (set to 0.15).

<sup>1</sup> Note that the original value of  $n_{\text{H,0}} = 0.67 \text{ cm}^{-3}$  quoted in Schaye et al. (2015) is incorrect. This error does not however affect any of the quoted values of  $f_{\text{th}}$  in that paper, with the mean and median values of  $f_{\text{th}}$  across the reference  $(100 \text{ Mpc})^3$  simulation being 1.06 and 0.7 respectively.

## 2.2 Subhalo identification and merger trees

Halo members are identified in the simulations first using a FoF algorithm, with a linking length set to 0.2 times the average inter-particle separation. Halo members are then divided into subhaloes using the SUBFIND algorithm (Springel et al. 2001; Dolag et al. 2009). Subhalo centers are set to the location of the particle with the lowest value of the gravitational potential. The subhalo within each FoF group with the lowest potential value is considered to be the central subhalo, and other subhaloes are referred to as satellites. For central subhaloes, we manually associate all particles within  $R_{\text{vir}} = R_{200,\text{crit}}$  to the subhalo for the purpose of computing accretion rates, etc, where  $R_{200,\text{crit}}$  is the radius enclosing a mean spherical overdensity equal to 200 times the critical density of the Universe. Accordingly, we quote halo masses as  $M_{200}$ , the mass contained within this radius.

We use merger trees constructed according to the algorithm described in detail in Jiang et al. (2014), with some additional post-processing steps that are described in Mitchell et al. (2020). The selection of the main progenitor of each subhalo is based on bijective matching between the  $N_{\text{link}}$  most-bound particles in each progenitor with those of the descendant, with  $10 \leq N_{\text{link}} \leq 100$ , depending on the total number of particles in each subhalo. This is then used to define the accretion rates of gas and dark matter that are associated with halo or galaxy merging events.

## 2.3 Measuring inflow rates with particle tracking

We measure inflow rates by tracking particles between consecutive simulation snapshots, exploiting the Lagrangian nature of the underlying SPH hydrodynamical scheme. We choose to measure inflow rates at two scales: the first being gas accretion onto haloes, and the second being gas accretion onto the ISM of galaxies. Inflow onto haloes is measured by identifying particles that cross the virial radius, and inflow onto galaxies involves identifying particles that join the ISM. Note that the inflow rates quoted in this study include only particles that join galaxies or haloes, and so do not represent the *net* inflow (inflow minus outflow) onto the system<sup>2</sup>.

We define the ISM as in Mitchell et al. (2020), including particles that are star forming, meaning they are both within 0.5 dex in temperature of the density-dependent temperature floor corresponding to the imposed equation of state, and that they also pass the metallicity-dependent density threshold given by Eqn. 1. We also include in the ISM any non-star-forming particles that are still within 0.5 dex of the temperature floor, and with density  $n_{\text{H}} > 0.01 \text{ cm}^{-3}$ , approximately mimicking a selection of neutral atomic hydrogen.

We measure whether inflowing particles are being recycled onto galaxies (or haloes) by first establishing if particles are ejected from the ISM of galaxies (or through the halo virial radius), following the procedure introduced and motivated by Mitchell et al. (2020). We impose a time-integrated radial velocity cut to select particles that are genuinely outflowing from the galaxy or from the halo (the instantaneous radial velocity is an unreliable predictor of whether particles will move outwards over a finite distance). Particles that fail this cut are not included in any later inflow measurement (neither first-time nor recycled). As a further detail, particles that fail the cut are given the opportunity to pass the cut (and so

join the outflow) at later snapshots, until they have either rejoined the ISM (or halo) or until three halo dynamical times have passed.

We use a fiducial time-integrated velocity cut of  $\frac{\Delta r_{21}}{\Delta t_{21}} > 0.25 V_{\text{max}}$ , where  $\Delta r_{21}$  is the radial distance moved between snapshots 1 and 2 by a particle that is first recorded as having left the ISM (or halo) at snapshot 1, and  $V_{\text{max}}$  is the subhalo maximum circular velocity. The time interval ( $\Delta t_{21}$ ) between snapshots 1 and 2 is held (as near as possible) constant to one quarter of a halo dynamical time, which mitigates the implicit dependence of outflow selection on the underlying snapshot spacing. In practice, the selection corresponds to a minimum radial displacement of  $\approx 15 \text{ kpc}$  for a halo mass of  $10^{12} M_{\odot}$  at  $z = 0$  (i.e. 7% of the halo virial radius, which is the case almost independently of halo mass, but changes to a slightly larger fraction of  $R_{200}$  at higher redshifts). The impact of changing this velocity cut by a factor two is minor, as demonstrated in Appendix B2.

Conceptually, this cut is implicitly making a distinction between small-scale ‘galactic fountain’ processes that occur at the disk-halo interface (scales out to a few tens of kpc for a Milky Way-mass galaxy) over timescales comparable to the galaxy dynamical time, and a larger-scale ‘halo fountain’ processes (tens to hundreds of kpc) that occur over timescales more comparable to a halo dynamical time (about one tenth of a Hubble time). Small-scale galactic fountains are poorly resolved in our analysis (due both to the finite time resolution of our simulation outputs, and to the limited spatial resolution of the simulations), and in any case act over timescales that are too short to have a significant direct impact on the efficiency with which galaxies form stars. As such our focus in this study is on wind recycling associated with the larger-scale halo fountain (and also on recycling of gas that moves outside the virial radius). Small-scale galactic fountains are of interest in other contexts, for example as a fine-grained mechanism to bring in mass and angular momentum from a hot corona (e.g. Fraternali 2017). Furthermore, observations of inflowing gas at the disk-halo interface (e.g. Bish et al. 2019) may be tracing smaller-scale galactic fountain processes that are either explicitly removed, or are unresolved, in our analysis.

Particles that leave galaxies (or haloes), and that pass the time-integrated velocity cut, are then tracked at later simulation snapshots, which enables us to establish if accreted particles are being accreted onto galaxies (or onto haloes) as:

- (i) first-time accretion,
- (ii) recycled accretion from a progenitor of the current galaxy (or halo),
- (iii) transferred accretion that was previously inside the ISM (or halo) of a non-progenitor galaxy (or halo).

We also compute the mass of gas that has been ejected from progenitors of the present galaxy (or halo), and that still currently resides outside the galaxy/halo. This is used to measure the characteristic efficiency of galaxy-scale and halo-scale wind recycling (see Section 3.3).

We also separate inflow rates between ‘smooth’ accretion (which can take the form of any of the three afore-mentioned accretion modes) and mergers. At the halo scale, particles that were inside the virial radius of a subhalo at the snapshot prior to being accreted onto the FoF group are considered as merging material. Note that this material can continue to be associated with satellite subhaloes, at least while they can still be identified in the simulation. Similarly, at the galaxy scale any gas that was inside the ISM of a non-main progenitor galaxy at the prior snapshot is considered as merging material. Any material that is not brought in by merg-

<sup>2</sup> Authors interested in the net inflow rates in EAGLE can obtain them by combining the results presented here with the outflow rates presented in Mitchell et al. (2020).

ers is instead considered “smooth” accretion. Note that for dark matter (which we only measure at the halo scale), “smooth” accretion is not an intrinsically well defined quantity, as essentially all dark matter would, if simulated at infinite numerical resolution, be accreted within haloes, depending precisely on the cutoff scale of the matter power spectrum, which in turn depends on the nature of the dark matter particle. Modern cosmological simulations typically only have the mass resolution to resolve  $\approx 50\%$  of the total mass in haloes (e.g. Springel et al. 2005; Genel et al. 2010; van Daalen & Schaye 2015). For gas, substantial true smooth accretion would be expected independent of numerical resolution, since after reionization the UVB (among other processes) provides indirect pressure support that both removes and prevents gas from ever being accreted onto very low-mass haloes.

Here, we define “smooth” accretion by setting an explicit fiducial halo mass cut at  $9.7 \times 10^8 M_\odot$ , corresponding to the mass of 100 dark matter (numerical) particles at fiducial EAGLE resolution. Gas or dark matter that is accreted onto a host halo while within another halo with mass lower than the limit are considered as smooth accretion. In addition, we do not track particles that are ejected from haloes (and their associated galaxies) below this mass scale, meaning that the limit also affects our definitions of first-time, recycled, and transferred (smooth) accretion. At the galaxy scale, we evaluate the maximum past mass of satellite subhaloes, and only count merging satellite galaxies to the merger accretion rate if the maximum past subhalo mass exceeds the cut. We assess the impact of varying our fiducial halo mass cut for smooth accretion in Appendix B3, and find that smooth gas accretion rates are generally well converged at the chosen mass cut (but would not have been if we had used a higher mass cut).

The methodology described here is similar in many respects to the methods employed by studies of gas inflow and wind recycling in cosmological zoom-in simulations (e.g. Übler et al. 2014; Christensen et al. 2016; Anglés-Alcázar et al. 2017; Grand et al. 2019). One noteworthy difference is in our definition of the distinction between “transferred” and “recycled” accretion, the potential importance of which has recently been highlighted by Anglés-Alcázar et al. (2017) and Grand et al. (2019). These authors implicitly consider “transfer” as consisting of particles that were ejected from any galaxy that is not flagged as the main progenitor of the descendant onto which the particles are now being accreted. Here, we instead define “recycled” accretion as particles that originated from any progenitor of the current galaxy (or halo), meaning that “transferred” accretion must originate from a non-progenitor galaxy. In practice, this means that gas that is ejected from satellites and then reaccreted after the satellite has merged with the host is tagged as recycled accretion in our scheme, but would be considered as transferred accretion in the afore-mentioned studies. While ultimately subjective, we regard our choice as being the more natural definition of wind recycling (distinct from “transfer”), since the definition of the main progenitor is often fairly arbitrary (though admittedly by low redshift a single main progenitor branch generally exists clearly within a merger tree), and the product of a galaxy merger should be considered as the sum of all progenitors. In addition, our definition of recycling naturally maps onto the framework of analytic and semi-analytic models, which generally merge the tracked ejected gas reservoirs of galaxies when they merge. We show the impact of this choice in Appendix B1 (our definition slightly increases the importance of recycling relative to transfer), and we take care to use consistent definitions when comparing to other simulations in Section 4.1.

Finally, we do not attempt to establish the physical reason for

why “transferred gas” is removed from a galaxy before being accreted onto another. Physical mechanisms may include feedback-driven outflows, ram pressure stripping against the corona of a massive host galaxy, or stripping by gravitational tides. Disentangling these effects is a non-trivial problem that sits outside the scope of our current study, but remains an interesting avenue for future work (see also Marasco et al. 2016 for work on stripping in EAGLE). Note that with our definition of “transferred” versus “recycled” accretion, gas that is stripped from satellites will be labelled as recycled accretion if the associated satellite merges before (or at the same time as) it is accreted onto the central galaxy, meaning that our definition of “transferred” gas may have a closer connection to feedback-driven outflows. We note also that when comparing our results to Grand et al. (2019), who are able to cleanly separate stripped versus feedback-driven transfer events due to their explicit wind model, we group these two components together for the purpose of the comparison.

### 3 RESULTS

Fig. 1 shows the total inflow rates of gas and dark matter onto haloes (top panel), as well as the total inflow rate of gas onto the ISM of galaxies (bottom panel), plotted as a function of halo mass. The values plotted here (and in all subsequent figures unless otherwise stated) are the average, which we compute (following Neistein et al. 2012; Mitchell et al. 2020) as the mean value of the numerator, divided by the mean value of denominator. This helps to ensure that the time-integral of the average inflow rates sum to the correct value of the average of the individual time-integrated rates. We compute averages by combining simulation snapshots in the redshift intervals indicated. Only central galaxies are included in the average (see van de Voort et al. 2017 for a detailed study of the differences between inflows onto centrals and satellites in EAGLE).

Fig. 1 shows the expected basic behaviour for gaseous inflow rates onto galaxies and haloes. At fixed mass, inflow rates increase with increasing redshift, reflecting the overall decline in the average density of the Universe with time. If we scale out the zeroth order time dependence by multiplying by the age of the Universe (not shown, but see Fig. 6), the redshift evolution is weaker, but there is still approximately 0.5 dex of evolution over  $0 < z < 5$ , with inflow rates still increasing with increasing redshift. Since dark matter haloes approximately grow at a rate that scales inversely with the Hubble time (at fixed mass), this implies that there may be additional processes beyond gravity alone that shape the redshift evolution of baryonic accretion onto galaxies and haloes in the simulation. In detail however, dark matter growth rates are not expected to scale exactly with the Hubble time (e.g. Correa et al. 2015), and indeed if we scale out the the age of the Universe, we do find that our measurements of dark matter accretion rates decrease by about 0.2 dex over the same redshift interval for which gas accretion rates decline by 0.5 dex. This implies therefore that there may also be effects related to pure gravitational evolution that affect the redshift evolution of gaseous inflow rates.

At fixed redshift, inflow rates increase with halo mass, both at the galaxy scale and at the halo scale. We choose to present results by first scaling out this zeroth order mass dependence, both to compress the dynamic range and also to highlight the important change in behaviour for galaxy-scale accretion at the characteristic halo mass of  $\sim 10^{12} M_\odot$  (see Correa et al. 2018a to view inflow rates in EAGLE without this rescaling). Normalised galaxy-scale inflow rates (bottom panel) clearly peak at (slightly below)

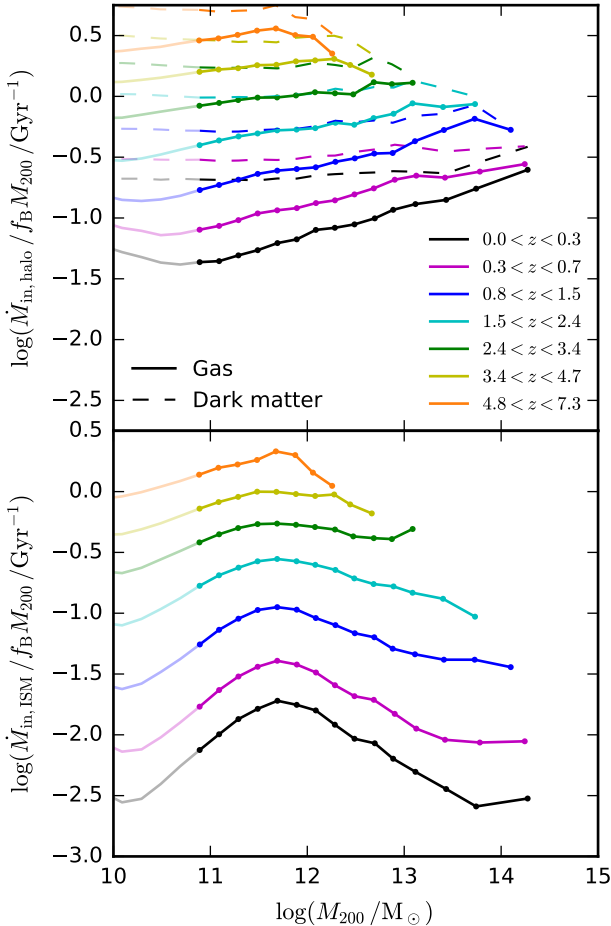


**Figure 1.** Gaseous inflow rates through the halo virial radius (top), and onto the ISM (bottom) of central galaxies, as a function of halo mass. Solid (dashed) lines show inflow rates for gas (dark matter). Inflow rates are normalised by  $f_B M_{200}$  for gas, and by  $(1 - f_B) M_{200}$  for dark matter, where  $f_B \equiv \frac{\Omega_B}{\Omega_m}$  is the cosmic baryon fraction, such that the normalised rates are equal if baryonic inflow perfectly traces the dark matter inflow rate at the virial radius. Inflow rates include contributions from smooth accretion and halo/galaxy mergers. Transparent lines indicate the range where there are fewer than 100 stellar particles per galaxy.

the mass scale of  $10^{12} M_\odot$  in EAGLE, though the feature becomes weaker with increasing redshift. The feature has a clear and obvious connection to the shape of the relationship between galaxy stellar mass and halo mass, in the sense that the ratio of stellar mass to halo mass also peaks strongly at the same characteristic halo mass (e.g. Behroozi et al. 2010; Moster et al. 2010). Interestingly, inflow rates at the halo scale do not show this peak (top panel), which aligns with the classic picture of galaxy formation in which longer radiative cooling timescales in high-mass haloes act to prevent coronal gas in the circum-galactic medium (CGM) from reaching the ISM, but not from being accreted onto the halo at the scale of the virial radius (e.g. Rees & Ostriker 1977), although the modern picture also requires effective AGN feedback to prevent a cooling flow (e.g. Bower et al. 2006; Croton et al. 2006), and these two ingredients may not be independent (Bower et al. 2017). Fig. 1 shows that gaseous inflow rates at the virial radius do however fall short of dark matter accretion rates (after scaling out the cosmic

baryon fraction) at lower halo masses. We return to this point in Section 3.1.

Fig 2 shows the relative contribution of smooth gaseous accretion, split between first-time infall, recycled infall (from progenitors of the current galaxy/halo), and transferred gas (from non-progenitors of the current galaxy/halo), as well as the contribution from mergers (at the halo scale this refers to the accretion of satellite subhaloes through the virial radius of the host). At both galaxy and halo scales, the single most important contributor to total gas accretion is generally provided by gas that is infalling for the first time. Mergers become an important source of gaseous accretion in higher-mass haloes ( $M_{200} \geq 10^{12} M_\odot$ ), especially at the galaxy scale (bottom panels). At the halo scale (top panels), recycling plays an important role at high halo masses, and actually provides the largest individual contribution for  $M_{200} > 10^{12} M_\odot$  in the low-redshift interval plotted. This trend is reversed at the galaxy scale however, with galaxy-scale recycling playing the largest role in lower-mass haloes ( $M_{200} \approx 10^{11} M_\odot$ ), and is subdominant in group and cluster mass haloes. Transferred accretion is negligible at the halo scale, aside from for very low-mass haloes ( $M_{200} < 10^{11} M_\odot$ ). Transferred accretion does play a role in higher mass haloes at the galaxy scale however, providing up to 20% of the total gas accretion for  $M_{200} > 10^{12} M_\odot$ .

While not shown, we have computed the mass fraction of stars that form in galaxies from the different accretion channels discussed here. In principle, stars may form from a biased sub-sample of the accreted gas; for example one could envisage that recycled gas is more metal enriched, and so more readily able to form stars. We find however that star formation associated with the different accretion channels closely tracks inflow rates onto galaxies, with no obvious bias favouring a particular accretion channel.

Putting this together, we find that all of the accretion channels considered play an important role for at least a subset of the various mass and spatial scales considered. Furthermore, we find that different individual accretion components scale in qualitatively distinct ways with halo mass (not shown for conciseness). For example, the peak in the total (halo mass normalised) galaxy-scale gaseous accretion rates seen in Fig. 1 at  $M_{200} \sim 10^{12} M_\odot$  is primarily created by the recycled and first-infalling components, and is not associated with the transfer and merging components. Overall, the situation is complex, reflecting the physics of radiative cooling and feedback on different scales. We now proceed to focus on isolating different parts of this picture in the following parts of this section.

### 3.1 Preventative feedback

The top panel of Fig. 1 shows that inflow rates at the virial radius fall short of dark matter accretion rates (after scaling out the cosmic baryon fraction) in low-mass haloes, with the discrepancy between the two growing with decreasing halo mass. At low redshift, the discrepancy actually becomes smaller at very low halo masses ( $M_{200} < 10^{11} M_\odot$ ), but this is the regime where galaxies are poorly resolved in EAGLE. This feature aside, the decline in gaseous inflow compared to dark matter inflow at lower halo masses can be attributed to the impact of feedback processes, as demonstrated explicitly in the recent dedicated study of halo-scale accretion in EAGLE by Wright et al. (2020). This “preventative feedback” effect (at the halo scale) has also been noted in studies of other cosmological simulations (Faucher-Giguère et al. 2011; van de Voort et al. 2011; Christensen et al. 2016; Mitchell et al. 2018; Tollet et al. 2019). Generally speaking, we find that EAGLE pre-

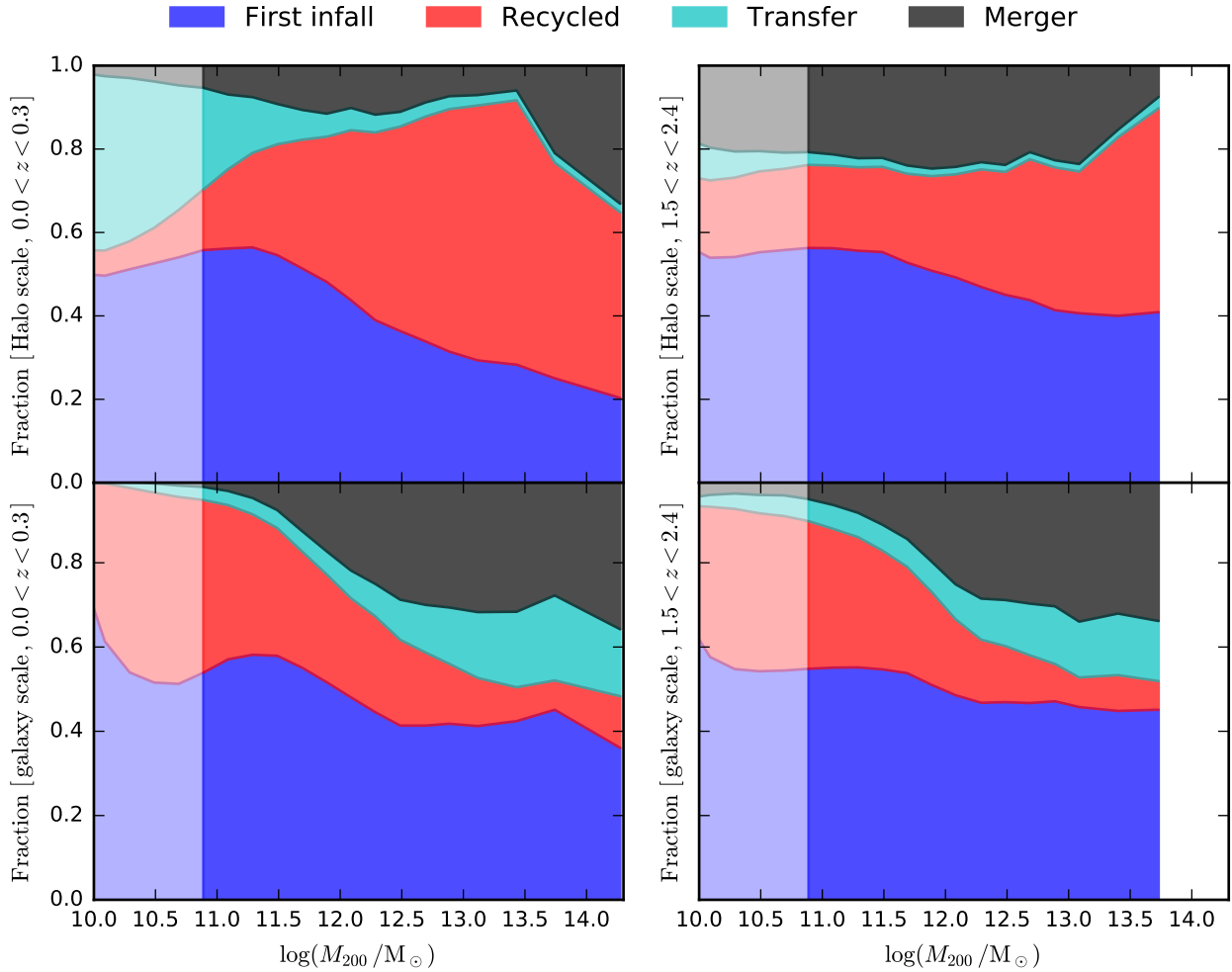


**Figure 2.** The fractional contribution of different inflow components to the total inflow rate onto haloes (top panels), and onto the ISM of central galaxies (bottom panels), as a function of halo mass. The coloured shaded regions show the contributions from first-infall (blue), recycling (i.e. from progenitors, red), transfer (i.e. from non-progenitors, cyan), and mergers (black). The definition of these components is distinct at the halo (top) and galaxy (bottom) scales, as described in the main text. Left (right) panels show averages for the redshift interval  $0 < z < 0.3$  ( $1.5 < z < 2.4$ ). The region with increased transparency indicates the halo mass range for which there are fewer than 100 stellar particles per galaxy.

dicts larger offsets between gaseous and dark matter accretion rates than in other simulations, most notably for haloes in the mass range  $10^{12} < M_{200}/M_{\odot} < 10^{13}$  (where there is no effect of feedback on halo-scale accretion in the OWLS simulations, for instance, van de Voort et al. 2011).

An important question, which has not (to our knowledge) been addressed in previous studies, is whether preventative feedback at the halo scale (if quantified as the ratio of the rates of total gas accretion to total dark matter accretion) reflects a reduction in smooth gas accretion onto haloes (either because of the ram pressure of outflows, or results from the thermal pressure injected into the CGM and intergalactic medium by feedback), or instead simply reflects the removal of baryons from progenitor haloes before they are accreted onto the main progenitor branch of the descendant halo (similar to the concept of pre-processing of satellite galaxies in group-mass haloes before falling into galaxy clusters, Bahé et al. 2013).

In Mitchell et al. (2020), we show that feedback drives large-scale outflows at the scale of the virial radius in EAGLE, which will indeed therefore reduce the baryon content of accreted satellite subhaloes before they are accreted through the virial radius

of the host. Here, we focus instead on the question of preventative feedback acting via the reduction of smooth gaseous accretion (defining smooth accretion as any gas or dark matter that enters the halo while **not** within the virial radius of a smaller halo of mass  $M_{200} > 9.7 \times 10^8 M_{\odot}$ , corresponding to 100 dark matter particles at standard EAGLE resolution).

The standard assumption for gaseous accretion (as exemplified for example by semi-analytic galaxy formation models) is that smoothly accreted gas that is being accreted onto a halo for the first time will trace the equivalent for dark matter. We therefore plot the ratio of first-time infall rates of gas and dark matter onto haloes in the top panel of Fig. 3, rescaling the dark matter rate by  $\Omega_b/(\Omega_m - \Omega_b)$ . The grey horizontal dashed line therefore indicates the expected value if gas traces dark matter. For low-mass haloes with  $M_{200} < 10^{11} M_{\odot}$ , we see that the ratio is below unity, implying that smooth gas accretion is indeed reduced compared to dark matter accretion. Intriguingly, the opposite is true for  $M_{200} > 10^{12} M_{\odot}$ , for which first-time infalling gas is being more efficiently accreted onto haloes, by up to 0.3 dex.

An alternative perspective on this is presented Fig. 4, which

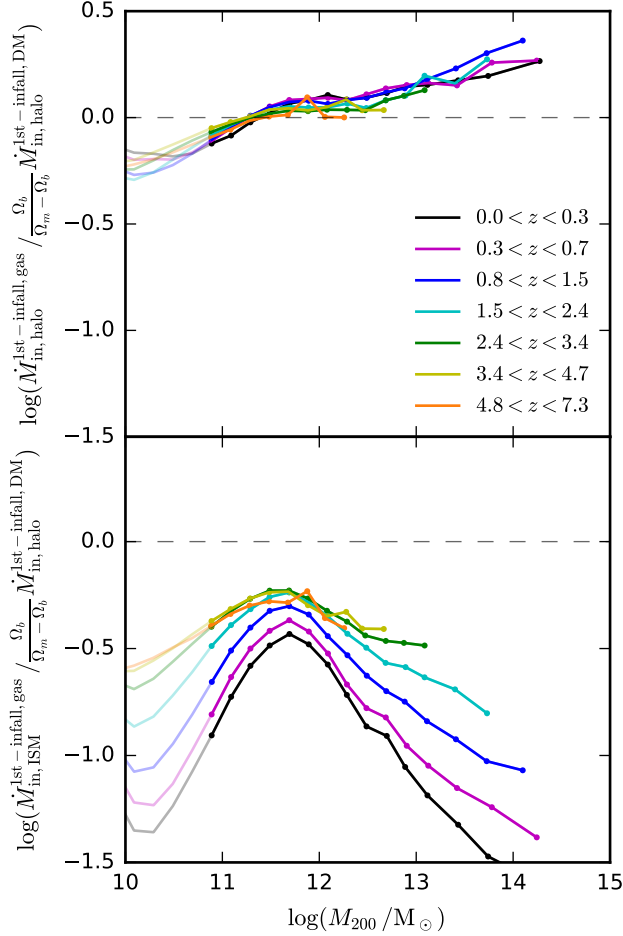


**Figure 3.** The ratio of the rates of smooth first-time gas inflow to smooth first-time dark matter inflow, as a function of halo mass. The top panel shows the ratio for gas to (scaled) dark matter inflow measured at the halo virial radius. The bottom panel shows the ratio of gas accretion rate onto the ISM of central galaxies, divided by the scaled dark matter inflow rate at the halo virial radius. Transparent lines indicate the range where there are fewer than 100 stellar particles per galaxy. At the virial radius, first-time gas accretion is slightly suppressed relative to first-time dark matter accretion at the virial radius for  $M_{200} < 10^{11} M_{\odot}$ , but is actually enhanced relative to dark matter accretion at higher masses (note however that total gas accretion rates are always comparable or lower than total dark matter accretion rates, see Fig. 1). First-time gas accretion onto the ISM of galaxies is always suppressed relative to first-time dark matter accretion at the virial radius, and more so at low-redshift, and at both low and high halo masses.

compares the cumulative masses of first-time infalling gas and dark matter, integrated in time over the entire merger tree of each descendant halo. Viewed in this way, there is still an enhancement of first-time gas accretion relative to dark matter in high-mass haloes ( $M_{200} \gtrsim 10^{13} M_{\odot}$ ), but the effect is weaker than seen in the instantaneous measure of preventative feedback presented in Fig. 3. Conversely, first-time gas accretion is more suppressed relative to dark matter accretion for low-mass haloes in the integrated measurement than for the instantaneous measurement (up to 0.4 dex for  $M_{200} \sim 10^{10} M_{\odot}$ ).

Fig. 5 then completes the picture by presenting the time evolution of the cumulative mass accretion of first-infalling gas and dark matter, again integrating over all progenitors of descendant haloes that are binned in mass at  $z = 0$ . Smooth first-time gas accretion

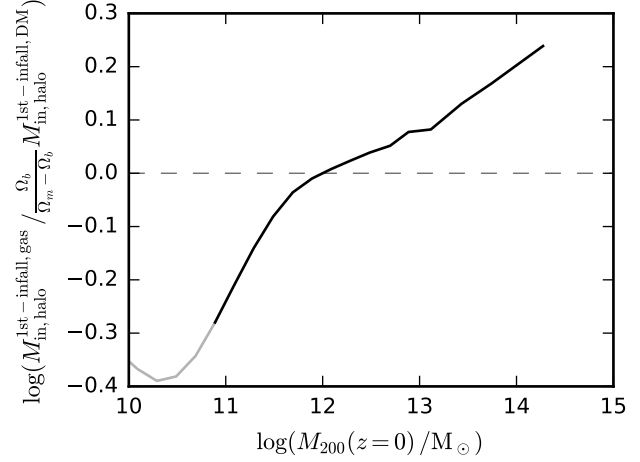


**Figure 4.** The ratio of masses of time-integrated first-time accreted gas over time-integrated first-time accreted dark matter, for matter accreted onto haloes by  $z = 0$ , as a function of the final halo mass. First-time accretion is computed across all progenitors of the final halo. Dark matter accretion is scaled by  $\frac{\Omega_b}{\Omega_m - \Omega_b}$ , and the grey horizontal dashed line indicates the expected value if gas traces dark matter. Transparent lines indicate the range where there are fewer than 100 stellar particles per galaxy. Integrated over the entire history of a halo, first-time gas accretion closely traces dark matter for  $M_{200} \sim 10^{12} M_{\odot}$ , is suppressed relative to dark matter accretion by up to 0.4 dex at lower halo masses, and exceeds dark matter accretion by 0.2 dex for  $M_{200} \sim 10^{14} M_{\odot}$ . The effect of preventative feedback is therefore stronger when integrated over the history of a halo, compared to the instantaneous view presented in Fig. 3.

is always suppressed relative to dark matter for the progenitors of haloes of mass  $M_{200}(z = 0) = 10^{11} M_{\odot}$ . At  $M_{200}(z = 0) = 10^{12} M_{\odot}$ , gas is delayed from being accreted onto the halo, rather than being prevented from entering (by  $z = 0$ ). This has the effect of shifting the peak redshift for instantaneous halo gas accretion rates (not shown) from  $z \approx 4$  (as for the dark matter) to  $z \approx 3$ . At  $M_{200}(z = 0) = 10^{13} M_{\odot}$ , gas accretion is reduced at high redshift, but the cumulative mass is slightly enhanced compared to that of dark matter for  $z < 2$ . We speculate that this could result from the enhanced radiative cooling rates that are possible once feedback enriches gas in the halo outskirts with heavy elements.

Preventative feedback has also been explored at the galaxy scale (e.g. Faucher-Giguère et al. 2011; van de Voort et al. 2011; Davé et al. 2012), at which point the term refers to the combined effects of feedback slowing or stopping the rates of gaseous infall on circum-galactic (and larger) scales, as well as the long-predicted effect that gas infall onto galaxies is restricted by long radiative cooling timescales in the coronae of high-mass haloes. The bottom panel of Fig. 3 presents an instantaneous measure of preventative feedback when framed in this way, plotting the ratio of first-time gaseous infall onto the ISM of galaxies, relative to the first-time infall of dark matter onto dark matter haloes. The results echo the trends seen in Fig. 1, showing that gas accretion onto galaxies peaks strongly at  $M_{200} \sim 10^{12} M_{\odot}$ . This partly reflects the afore-mentioned preventative feedback at the virial radius, but also reflects the efficiency with which gas is able to infall from the CGM (within the virial radius) down onto the ISM. We separate the latter effect in the next section.



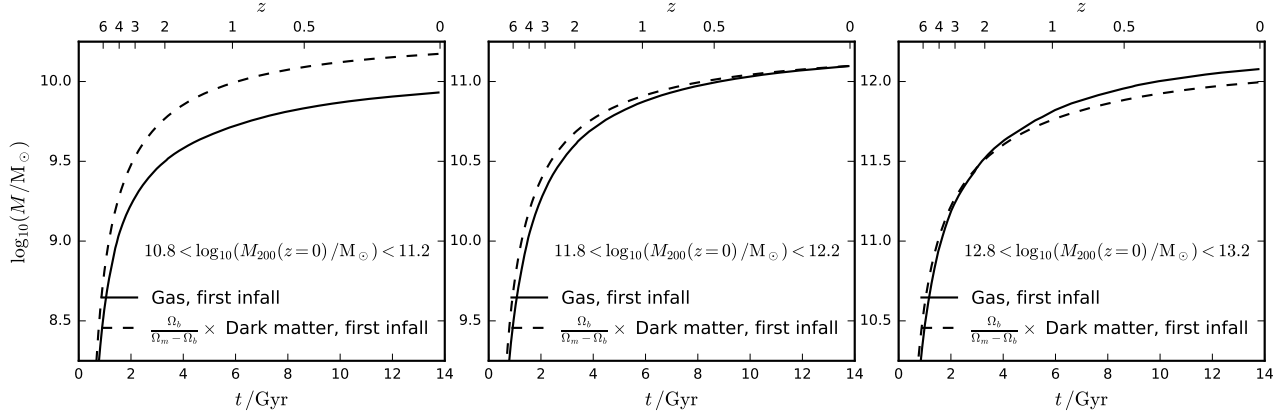


**Figure 5.** The evolution of cumulative mass in first-time accreted gas (solid) and dark matter (dashed) onto haloes, binned by the final halo mass at  $z = 0$ , as labelled. First-time accretion is computed across all progenitors of the final halo. Dark matter accretion is scaled by  $\frac{\Omega_b}{\Omega_m - \Omega_b}$ . For the  $M_{200}(z = 0) = 10^{11} M_\odot$  bin (left panel), gas accretion is consistently suppressed relative to dark matter for all but the earliest times. For the higher halo mass bins, gas accretion rates are suppressed relative to dark matter at high redshift, but are enhanced relative to dark matter at lower redshifts. For the  $M_{200}(z = 0) = 10^{12} M_\odot$  bin (middle panel), this has the outcome that the cumulative first-time gaseous and dark matter accretion balance by  $z = 0$ . Feedback therefore has the effect of (slightly) delaying gas accretion onto haloes for this mass range, without preventing any of the total expected amount of gas accretion by  $z = 0$ .

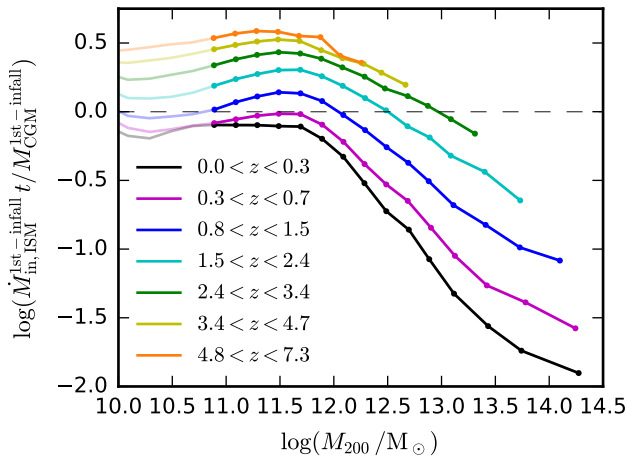


**Figure 6.** Accretion rates of gas inflowing for the first time onto the ISM of central galaxies, normalised by the mass in the CGM out to the virial radius, as a function of halo mass. For both quantities, only gas that has never been in the ISM of a galaxy is included. We also scale out the age of the Universe,  $t$ , at each redshift. With the chosen normalisation, the normalised inflow rates define a dimensionless efficiency for gas to infall from the CGM onto the ISM for the first time (a value of unity implies that gas infalls over a Hubble time). Transparent lines indicate the range where there are fewer than 100 stellar particles per galaxy. The infall efficiency increases weakly with halo mass for  $M_{200} < 10^{12} M_\odot$ , peaking slightly at this mass, and then strongly decreases with halo mass for  $M_{200} > 10^{12} M_\odot$ . This reflects the transition from short to long radiative cooling times due to the shift of the virial temperature beyond the peak of the cooling curve, and the effect of AGN feedback.

### 3.2 Infall from the CGM

Fig. 6 presents the efficiency of first-time gaseous infall from the CGM onto the ISM. We define this efficiency as  $\dot{M}_{\text{in,ISM}}^{\text{1st-infall}} / M_{\text{CGM}}^{\text{1st-infall}}$ , where  $\dot{M}_{\text{in,ISM}}^{\text{1st-infall}}$  is the inflow rate of gas onto the ISM for gas that has never been in the ISM of a galaxy before, and  $M_{\text{CGM}}^{\text{1st-infall}}$  is the mass of gas in the CGM (by which we mean outside the ISM but within the halo virial radius) of the

central subhalo, and that also has never been in the ISM of a galaxy before. This efficiency is the inverse of the characteristic timescale for the first-infalling gas in the CGM to be depleted onto the ISM (exactly analogous to the standard definition of the gas depletion time in the ISM, for example). We then scale out the zeroth order time dependence by multiplying by the age of the Universe, which defines a dimensionless efficiency of first-time CGM infall.

Fig. 6 shows that the efficiency of first-time infall from the CGM is nearly (but not completely) independent of halo mass for  $M_{200} < 10^{12} M_\odot$ , but declines strongly with increasing halo mass for  $M_{200} > 10^{12} M_\odot$ . This again reflects the classic anticipated dichotomy in galaxy formation between a regime in which infall is limited primarily by gravitational timescales (which are scale free, and so independent of halo mass) in low-mass haloes, to a regime where infall is limited by radiative cooling timescales (which are strongly scale dependent, due to atomic physics) and AGN feedback. Intriguingly, the efficiency of first-time infall does peak slightly at  $\sim 10^{12} M_\odot$  at higher redshifts (but not at  $z = 0$ ), indicating that there may be more than just gravity regulating infall, even in the limit of short cooling times. Galaxy star formation rates, and therefore outflow rates, also increase strongly with increasing redshift (e.g. Mitchell et al. 2020), and so we speculate that the slight decrease in the first-time infall efficiency with decreasing halo mass for  $M_{200} < 10^{12} M_\odot$  for  $z > 1$  could be related to feedback processes. This is however a smaller effect compared to the modulation of first-time infall on larger scales discussed in Section 3.1, implying that feedback may primarily regulate first-time gas infall on larger spatial scales.

This can be rationalised by supposing that gas inflow rates in low-mass haloes are comparatively less affected by feedback in the inner CGM, as outflows propagate perpendicular to the disk (which we have shown to the case in EAGLE, Mitchell et al. 2020), away from the primary plane of small-scale inflow, while outflows and inflows are more isotropic (and so can more readily interact) on larger scales beyond the virial radius. Note that galactic winds do evacuate significant amounts of gas out of the halo virial radius (most of which has never been in the ISM before), affecting the denominator of our defined infall efficiency. As seen in the lower-right panel of figure 1 in Mitchell et al. (2020), the (halo mass-normalised) out-

flow rate at the virial radius is approximately independent of halo mass, meaning that this effect will not affect the halo-mass dependence of the infall efficiency shown here.

Considering instead the redshift evolution of the first-time infall efficiency, Fig. 6 shows that even after scaling out the zeroth order time dependence, there is still about 0.5 dex of evolution at fixed mass over the interval  $0 < z < 3$ . This is contrary to the expectation that (in the regime of short radiative cooling times) gas infalls from the CGM over a gravitational freefall timescale, since this timescale scales approximately with the halo dynamical time ( $t_{\text{dyn}} \equiv R_{\text{vir}}/V_{\text{circ}}$ , where  $V_{\text{circ}}$  is the halo circular velocity at  $R_{\text{vir}}$ ), which itself is approximately 10% of the Hubble time at a given redshift. The decrease in the infall efficiency with decreasing redshift could reflect the increase in specific angular momentum with decreasing redshift at fixed halo mass (providing more rotational support against collapse to the center), or could be related to the impact of feedback processes, either by reducing inflow rates directly (numerator of the infall efficiency), or by altering the overall mass reservoir of the CGM (denominator of the infall efficiency). At higher halo masses, where radiative cooling is expected to provide the limiting timescale, lower infall efficiencies can be straightforwardly explained by the lower average densities at low-redshift (e.g. Correa et al. 2018a).

### 3.3 Galactic and halo-scale wind recycling

We parametrise the efficiency of recycling for gas that is ejected from galaxies and haloes by measuring  $\dot{M}_{\text{in}}^{\text{recycled}}/M_{\text{ej}}$ , where  $\dot{M}_{\text{in}}^{\text{recycled}}$  is the rate of return of recycled gas, and  $M_{\text{ej}}$  is the instantaneous mass of the reservoir of ejected gas (which is currently located outside the galaxy or halo). This definition gives the inverse of the depletion time for the ejected gas reservoir. We then scale out the zeroth order time dependence by multiplying by the age of the Universe, yielding a dimensionless efficiency. We provide measurements at both galaxy and halo scales. The galaxy-scale measurement includes gas that has been ejected from the ISM of galaxies (irrespective of whether that gas is also ejected through the virial radius). The halo-scale measurement includes gas that has been ejected beyond the halo virial radius (in this case irrespective of whether that gas has ever been situated inside the ISM of a galaxy in the past). Note that the halo-scale measurement is equivalent to the definition that is generally used in semi-analytic galaxy formation models; we compare our measurements with the values adopted in such models in Section 4.3.1.

The measurements of wind recycling efficiency are presented in Fig. 7. At the halo scale (top panel), the recycling efficiency always increases with halo mass, approximately as  $\dot{M}_{\text{in}}^{\text{recycled}}/M_{\text{ej}} \propto M_{200}^{0.6}$  at  $z = 0$ . At the galaxy scale (bottom panel), the recycling efficiency peaks at the characteristic mass scale of  $10^{12} M_{\odot}$ . At a fixed halo mass of  $M_{200} = 10^{12} M_{\odot}$ , the dimensionless efficiency of recycling (at both galaxy and halo scales) decreases by nearly one order of magnitude from  $z = 3$  to  $z = 0$ . At higher redshifts, the halo-scale efficiency continues to increase, but there is no longer any clear evolution at the galaxy scale.

Comparing the two recycling efficiencies, recycling is much more efficient at the halo scale than at the galaxy scale for  $M_{200} > 10^{12} M_{\odot}$ , but is more comparable at lower halo masses. Compared to the efficiency corresponding to characteristic gas return over a Hubble time (a value of unity, shown by the dashed horizontal lines), the gas ejected at the halo scale typically returns after a halo dynamical time (about one tenth of the age of the Universe) for  $M_{200} \approx 10^{13.5} M_{\odot}$ , and returns after a Hubble time for

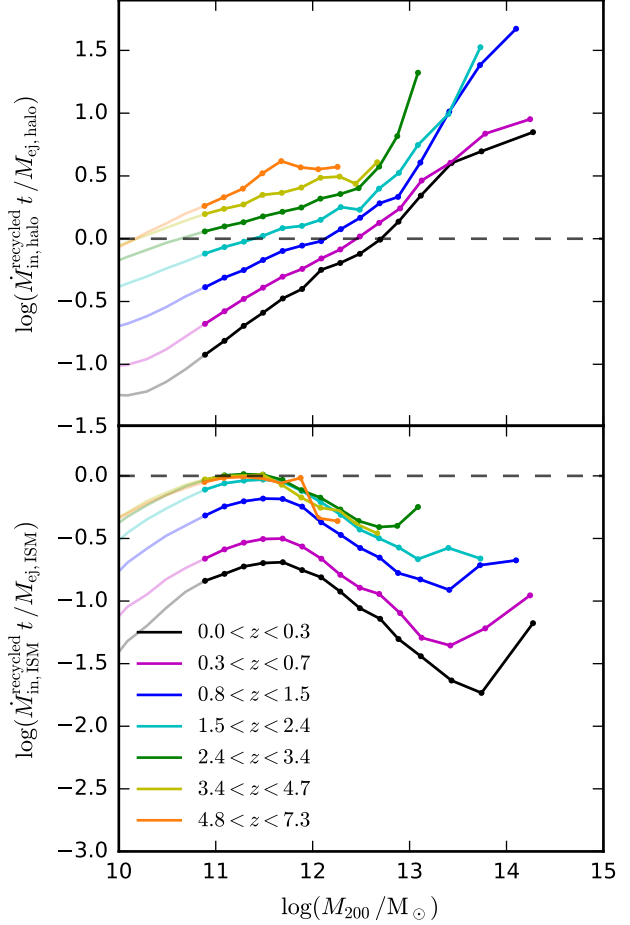


**Figure 7.** Inflow rates of recycled gas through the halo virial radius (top panel), and onto the ISM of central galaxies (bottom panel), as a function of halo mass. The inflow rates in the top (bottom) panel are normalised by the mass of material that has been ejected from progenitor haloes (galaxies), and that still currently resides outside the virial radius (ISM) at the plotted redshift. Inflow rates are multiplied by the age of the Universe at each redshift, altogether defining a dimensionless efficiency of wind recycling at the halo or galaxy scale. Transparent lines indicate the range where there are fewer than 100 stellar particles per galaxy. At  $z = 0$ , halo-scale gas recycling is relatively efficient (timescales shorter than a Hubble time) for  $M_{200} > 10^{13} M_{\odot}$  at  $z = 0$ , but is inefficient for lower-mass haloes. Halo gas recycling becomes more efficient at higher redshifts. Gas recycling onto galaxies is inefficient (timescales equal or longer than a Hubble time) for all masses/redshifts, and the efficiency peaks at  $M_{200} \sim 10^{11.7} M_{\odot}$ .

$M_{200} \approx 10^{12} M_{\odot}$  at  $z = 1$ . At the galaxy scale, ejected gas on average returns over a timescale that is equal or longer than the Hubble time for all halo masses, reaching up to ten times the Hubble time at  $M_{200} \approx 10^{10} M_{\odot}$  and at  $M_{200} \approx 10^{13} M_{\odot}$ . Note however that despite the very low efficiency of galaxy-scale wind recycling, this still forms an important contribution to galaxy-scale inflow rates, especially for  $M_{200} \sim 10^{11} M_{\odot}$  (Fig. 2). This reflects the global inefficiency of gaseous inflow onto galaxies in the simulation.

Importantly, much of the gas that is ejected from the galaxies in EAGLE is also ejected beyond the halo virial radius. As such, the low efficiency we find for galaxy-scale wind recycling does not necessarily imply that recycling is inefficient for the subset of gas that is retained inside of the virial radius. This is demonstrated in

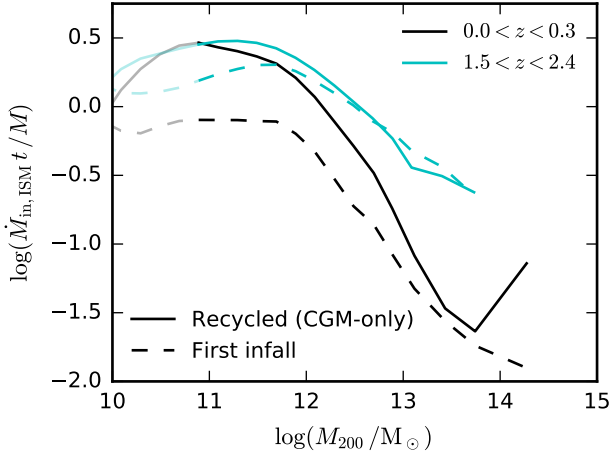


**Figure 8.** The dimensionless efficiency of galaxy-scale wind recycling (solid lines), in this case measured relative to the subset of ejected gas that is still located within the halo virial radius, with mass  $M_{\text{ej}}(r < R_{200})$ . We define the efficiency in this case as  $\dot{M}_{\text{in,ISM}}^{\text{recycled}} t / M_{\text{ej}}(r < R_{200})$ , where  $\dot{M}_{\text{in}}^{\text{recycled}}$  is the inflow rate of recycled gas onto the ISM, and  $t$  is the age of the Universe. As a reference, we overplot the efficiency of first-time infall from the CGM onto the ISM (dashed lines), defined as  $\dot{M}_{\text{in,ISM}}^{\text{1st-infall}} t / M_{\text{CGM}}^{\text{1st-infall}}$ , as introduced in Fig. 6. While global galaxy-scale gas recycling is always inefficient in EAGLE (Fig. 7), ejected gas that is still within  $R_{200}$  is recycled more efficiently, with an efficiency that is comparable or greater than that of first-time infall.

Fig. 8, which shows an alternative measure of the dimensionless efficiency of galaxy-scale wind recycling, in this case defined as  $\dot{M}_{\text{in,ISM}}^{\text{recycled}} t / M_{\text{ej}}(r < R_{200})$ , where  $M_{\text{ej}}(r < R_{200})$  is now the mass of ejected gas that is still within  $R_{200}$ . Defined in this way, recycling of circum-galactic gas onto the ISM (solid lines) is actually comparable or greater (by up to 0.5 dex) in efficiency than that of first-time infall from the CGM (as introduced in Section 3.2, and shown as dashed lines here for comparison). This illustrates that a subset of the gas that is ejected from the ISM in EAGLE is being efficiently (at least comparatively) recycled in a fountain flow.

As an aside, we note that semi-analytic galaxy formation models often implicitly assume that the efficiency of infall from the CGM (within the virial radius) onto the ISM is the same for recycled and first-infalling gas. Specifically, these models typically assume that “reincorporated” ejected gas should be placed back in the total reservoir of gas within  $R_{200}$ , which can then infall onto the ISM with a single efficiency. Fig. 8 shows that this is not an unreasonable assumption, since the efficiency of CGM-scale recycling and first-infall are qualitatively similar. Quantitatively, it may be worthwhile for galaxy formation models to account for the possibility that recycled gas is able to infall back onto the ISM with a higher efficiency than that of gas that is infalling for the first time, particularly by low-redshift. Note that as discussed in Section 2.3, our definition of galactic outflows (which are required to move outwards a given distance over a given interval) means that this relatively high recycling efficiency is associated with a fountain that, for the case of a Milky Way-mass halo at low redshift, generally extends over scales of many tens of kpc, as opposed to a small-scale galactic fountain that operates on scales of 10 kpc or less.

Fig. 9 presents the cumulative residency time (time since ejection) distributions for ejected gas that is currently (i.e. at the redshift indicated) being recycled onto haloes (top panel), or onto the ISM of central galaxies (bottom panel). As before, the halo-scale resi-

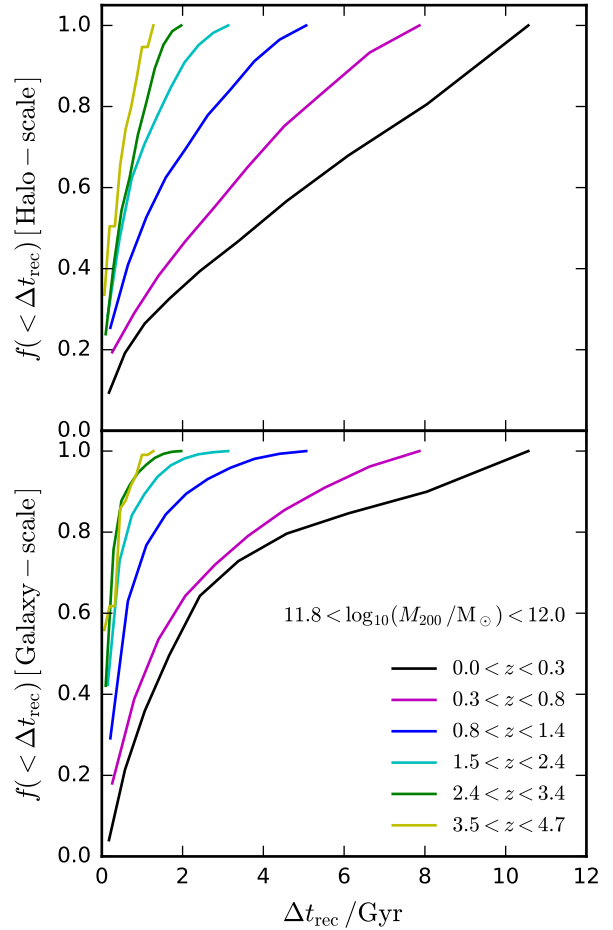


**Figure 9.** The cumulative distribution of gas return timescales for gas being recycled at the indicated redshifts, having been ejected at a time  $\Delta t_{\text{recycle}}$  in the past. The top (bottom) panel shows recycling onto haloes (the ISM of central galaxies), selected with  $10^{11.8} < M_{200} / M_{\odot} < 10^{12}$ . The distributions are plotted as the mean for the redshift bins indicated. The median return timescale of returning gas decreases with redshift, and is always shorter (and with a narrower distribution) at the galaxy scale than at the halo scale.

dency time distribution includes gas irrespective of whether it was ejected from the ISM of a galaxy in the past. Distributions are plotted for a fixed halo mass range of  $10^{11.8} < M_{200} / M_{\odot} < 10^{12}$ .

At the galaxy scale, the median recycling time at  $0 < z < 0.3$  is 1.7 Gyr. Note that this only accounts for returning gas, unlike the definition of the characteristic return time plotted in Figs. 7 and 8. The median recycling time depends strongly on redshift, reducing to 480 Myr by  $z = 1$ , and to 230 Myr by  $z = 2$ . This evolution reflects the evolution of the characteristic halo dynamical time (which in turn shapes characteristic gravitational freefall timescale), but may also reflect the development of a hot, pressurized gaseous halo by low redshift, which could plausibly lengthen recycling times. Median recycling times are longer at the halo scale (3.9 Gyr at  $0 < z < 0.3$ ), and the distributions are broader, with a larger fraction of gas returning after having been ejected from the halo at high redshift.

Finally, Fig. 10 presents the cumulative distributions of distances reached by ejected gas that is either currently (i.e. at the redshift indicated) returning to the halo (top-right) or galaxy (bottom-

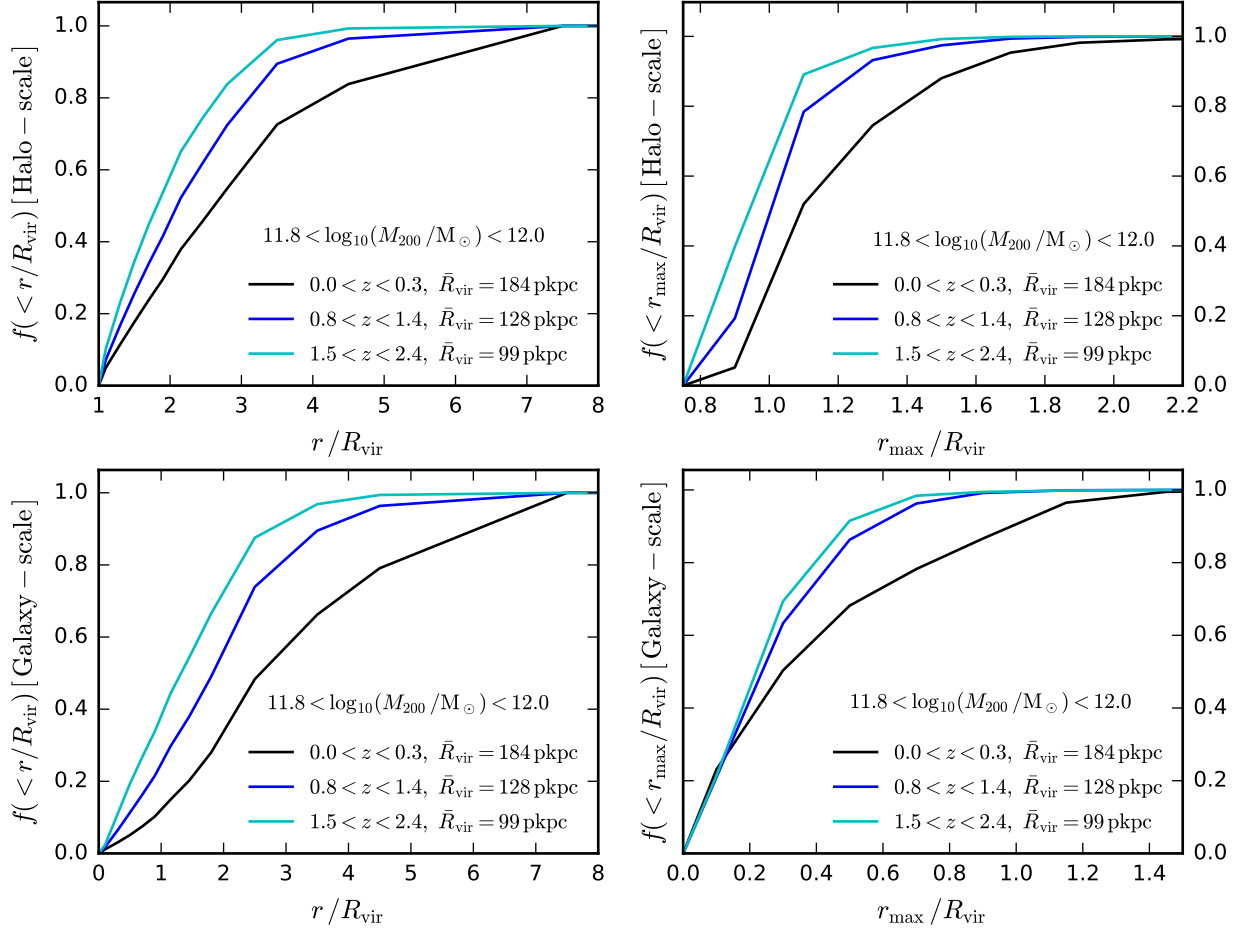


**Figure 10.** The cumulative distributions of radius for gas ejected from haloes (top panels) and galaxies (bottom panels) for haloes with masses in the range  $11.8 < \log_{10}(M_{200}/M_{\odot}) < 12$  at the redshifts indicated. Left panels show the positions of ejected particles that have not returned to the halo/galaxy at the indicated redshift. Right panels show the maximum past radius of returning particles. In both cases radii are normalised by the median value of the halo virial radius ( $\bar{R}_{\text{vir}}$ ) at each redshift interval plotted. Most of the gas ejected from galaxies resides beyond the virial radius (bottom-right panel), but most of the gas recycled onto galaxies was not ejected outside of the halo (bottom-right panel). Gas ejected from haloes (top-left panel) sits at roughly the same median position (median value  $\approx 2R_{\text{vir}}$  at  $z \approx 0$ ) as gas ejected from galaxies (bottom-left panel).

right), or is currently residing outside the halo (top-left) or galaxy (bottom-left). Distributions are plotted for three redshift bins with a fixed halo mass of  $10^{11.8} < M_{200}/M_{\odot} < 10^{12}$ . For returning gas (right panels), the distance plotted is the maximum radius achieved, normalised to the current value of the halo virial radius. For resident ejected gas (left panels), the distance plotted is the current radius, normalised again to the current value of the halo virial radius (for the halo from which the gas was ejected).

Most of the gas ejected from the ISM of galaxies resides beyond the virial radius (bottom-left panel). For the plotted halo mass range, the median radius of resident ejected gas is  $2.6 R_{\text{vir}}$  for  $0 < z < 0.3$ , decreasing to  $1.8 R_{\text{vir}}$  for  $0.8 < z < 1.4$ , and to  $1.3 R_{\text{vir}}$  for  $1.5 < z < 2$ . Only 12% of the resident ejected gas is inside the virial radius for  $0 < z < 0.3$ , though this fraction increases to 25% by  $0.8 < z < 1.4$ , and to 37% by  $1.5 < z < 2$ . The median distances of gas that has been ejected from haloes (irrespective of having been in the ISM, top-left panel) are similar. The maximum distance ever recorded for ejected gas (either from galaxies or from haloes) is  $\approx 1.3$  pMpc for the plotted halo mass range.

For gas that is being recycled onto haloes (top-right) or galaxies (bottom-right), the maximum distances achieved are much smaller. At the halo scale, the median distance achieved is only  $1.1 R_{\text{vir}}$  for  $0 < z < 1.3$ , and essentially all of the returning gas has  $r_{\text{max}} < 2 R_{\text{vir}}$ . Note that it is possible for returning gas to have  $r_{\text{max}} < R_{\text{vir}}$ ; this reflects the growth of the halo virial radius with time (the virial radius quoted is the value just after gas has been recycled). Note also that this gas must spend a significant amount of time outside the halo, due to our adopted time-integrated velocity cuts, see Section 2.3. At the galaxy scale (bottom-right), returning gas has generally never left the halo. The median maximum distance achieved is  $0.3 R_{\text{vir}}$  at  $0 < z < 0.3$ , corresponding to a fountain flow on scales of several tens of pkpc. Note again that there is expected to be another gaseous component that participates in a smaller-scale galactic fountain (over shorter timescales), which is excluded from our measurements (see Section 2.3).

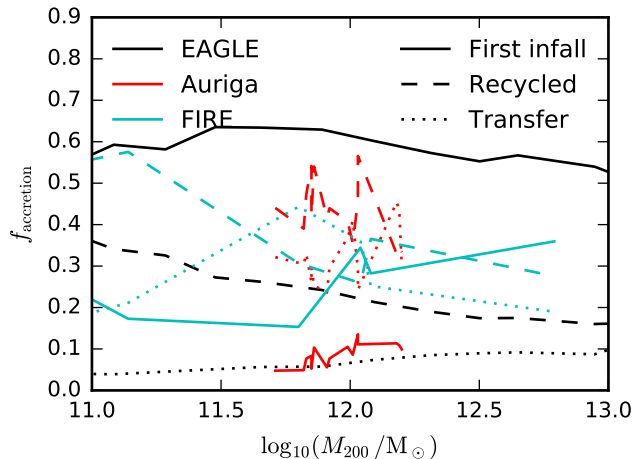


**Figure 11.** The fraction of the final stellar mass contributed by different accretion channels at  $z = 0$ , as a function of halo mass. Contributions are plotted for the “First infall” (solid), “Recycled” (dashed), and “Transfer” (dotted) channels, as defined in the main text. We compare results from the reference EAGLE simulation (black) with results from cosmological zoom-in simulation projects, including Auriga (red, Grand et al. 2019) and FIRE (cyan, Anglés-Alcázar et al. 2017). Generally speaking, galaxies in EAGLE are assembled mostly from first-infalling gas, whereas in Auriga galaxies are assembled mostly by gas that has been ejected and then recycled at least once. Over the same mass range as spanned by Auriga, FIRE galaxies present an intermediate scenario, but with a stronger emphasis on transferred accretion.

## 4 LITERATURE COMPARISON

### 4.1 First-time, recycled, and transferred inflow fractions

We now consider how our results from EAGLE compare to measurements presented in the literature using other cosmological simulations, each of which uses a different implementation of subgrid physics for star formation and feedback. We focus primarily here on the importance and efficiency of wind recycling. Fig. 11 compares the fractional contributions of first-time, recycled, and transferred gaseous inflow to the stellar mass of galaxies between EAGLE, and zoom-in simulations from the Auriga (Grand et al. 2017) and FIRE simulation projects (Hopkins et al. 2014). For the cases of Auriga and FIRE, this fraction corresponds to the fraction of the final stellar mass of  $z = 0$  galaxies. We use almost exactly the same definition for EAGLE, but in our case the fraction is computed by integrating over the star formation history of all progenitor galaxies, and is therefore weighted instead by the initial stellar mass of particles before stellar mass loss (we do not expect this to bias our results significantly for galaxies at  $z = 0$ ). To be consistent with the other studies, we use the main progenitor to define the dichotomy between transferred and recycled gas for the comparison (see Section 2.3).

While we take these steps in order to make our measurements as comparable to the others as is reasonably possible, it should be noted that there are still differences in the methodologies used. Relative to our velocity cuts, Anglés-Alcázar et al. (2017) use different velocity cuts to define ejected gas in FIRE (relying on the instantaneous rather than time-integrated velocity). We show in Appendix B2 that the recycling is fairly insensitive to the velocity cut used, and Anglés-Alcázar et al. (2017) arrive at the same conclusion after varying their cuts, and so we do not expect this to affect the qualitative conclusions drawn from the comparison. The stellar

feedback scheme of Auriga utilises hydrodynamically decoupled wind particles, which enables the explicit identification of which gas tracers in their simulations have been ejected from the ISM by stellar feedback, removing the need for any velocity cuts. The characteristic maximum distance achieved by recycled wind particles in Auriga is  $\approx 20$  kpc (independent of redshift), which is uncomfortably close to the minimum allowed distance  $\approx 15$  kpc implied by our velocity cuts for a Milky Way-mass halo at low redshift (though our velocity cuts would correspond to smaller maximal distances for Milky Way progenitor haloes at higher redshifts). As mentioned previously, decreasing the velocity cut by a factor two (and so halving the minimum allowed distance to be considered recycling) has little impact on our results (Appendix B2)<sup>3</sup>. It is still important to acknowledge that smaller-scale galactic fountain processes may occur in reality however.

The explicit wind particle scheme of Auriga also allows Grand et al. (2019) to distinguish between gas that is removed from the ISM by feedback as opposed to stripping processes (gravitational tides or ram pressure). Since neither we nor Anglés-Alcázar et al. (2017) attempt to make this distinction, we group the stripped and feedback-transferred components of Grand et al. (2019) into a single “transfer” component for comparative purposes.

A final issue that could affect comparing EAGLE with zoom-in simulations is that EAGLE utilises lower resolution. This is potentially important for the fraction of recycled and transferred accretion, since EAGLE may not resolve the ISM of very low-mass progenitor galaxies. While very low-mass progenitor/satellite galaxies are negligible in terms of their stellar mass, and are naturally truncated by the preventative feedback associated with photo-heating from the UVB, they are not necessarily negligible in terms of the combined cumulative mass in outflows, since outflow rates per unit star formation increase strongly with decreasing stellar mass (e.g. Muratov et al. 2015; Mitchell et al. 2020). Using a higher-resolution simulation, we explore the effect of varying our fiducial halo mass cut (above which we track ejected gas, and so count later recycling and transfer) in Appendix B3, and find that the contribution of recycled and transferred gas is reasonably well converged for our fiducial mass cut.

Bearing these caveats in mind, Fig. 11 shows that EAGLE predicts a significantly higher contribution from first-infalling gas accretion, roughly 60%, relative to recycling when compared to the Auriga simulations, roughly 10%. Based on the various checks we have performed, we expect this conclusion to be qualitatively robust, and we interpret the difference as being caused by the different implementations of stellar feedback between the simulations. In Auriga, gas is ejected from galaxies by stellar feedback by explicit wind particles that are temporarily decoupled from the hydrodynamical scheme, and which typically recouple before reaching 10 kpc in distance, which is close to the average distance of 20 kpc achieved by recycled particles (Grand et al. 2019). In Mitchell et al. (2020), we compare outflow rates at different spatial scales with the Illustris-TNG simulation (Nelson et al. 2019), which uses a very similar implementation of stellar feedback as Auriga. There, we show that EAGLE drives outflows over much larger spatial scales

<sup>3</sup> If we instead remove all velocity cuts, the contribution of recycling would increase significantly (up to 50 – 60%), but still not to the extent that Auriga and EAGLE would come into agreement for the contribution of first-infalling gas. From visual inspection of particle trajectories, we believe that the increase in EAGLE recycling rates for this case is more related to particles fluctuating across the phase boundary defining the ISM, rather than reflecting genuine feedback-driven outflows however.

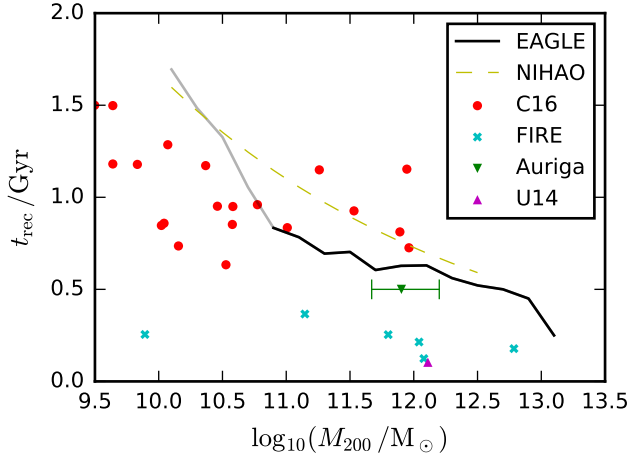


**Figure 12.** The median residency time of returning gas after being ejected from the ISM of central galaxies over the redshift range  $0 < z < 3$ . Note that this measurement excludes gas that does not return by  $z = 0$ . We compare results from the reference EAGLE simulation (black) with results from cosmological zoom-in simulation projects, including Auriga (green, Grand et al. 2019), FIRE (cyan, Anglés-Alcázar et al. 2017), NIHAO (yellow, Tollet et al. 2019), and the zoom-in simulations of Christensen et al. (2016), C16, red) and Übler et al. (2014, U14, magenta). For EAGLE, we indicate in grey the halo mass range for which galaxies contain fewer than 100 stellar particles. With the exception of the measurements from FIRE and U14, both of whom find short recycling timescales, there is good consensus among simulations that gas returns to galaxies over a timescale between 0.5 to 1 Gyr for  $M_{200} > 10^{11} M_{\odot}$ , and takes longer than 1 Gyr to return at lower masses. We emphasise, however, that because this timescale excludes the contribution of non-returning particles, it is not a particularly useful way to characterise the efficiency of wind recycling.

at fixed mass (in the mass range where stellar feedback dominates) than in Illustris-TNG. This is consistent with the qualitative differences in the importance of first-time versus recycled gaseous accretion between EAGLE and Auriga, in the sense that recycling is less efficient in EAGLE.

Roughly speaking, the FIRE simulations present a scenario that is intermediate between the EAGLE and Auriga cases (about 30% from first-time accretion), albeit with significant object-to-object scatter, and with a larger contribution from the transferred component. Other studies find similarly intermediate results between EAGLE and Auriga: Christensen et al. (2016) report that between 20% and 40% of gas accretion onto galaxies is recycled in their zoom-in simulations, and Übler et al. (2014) find  $\approx 45\%$  of the gas accretion is first-time accretion. Note that these latter studies do not separate transferred accretion (and so we do not show them directly in Fig. 11).

## 4.2 Recycling residency times

Most studies of wind recycling with cosmological simulations in the literature have characterised recycling with the residency time for returning gas, i.e. the time between ejection and return. In some cases the median residency time is further taken as a measure of the efficiency of wind recycling, and is then compared to the parameterisations used in analytic and semi-analytic galaxy formation models. The flaw with this approach is that it neglects the contribution of gas that has not returned by  $z = 0$ , and so does not correctly

characterise the recycling efficiency if the fraction of non-returning gas is significant.

We compare the median residency time for gas that has been ejected from (and then returned to) the ISM of galaxies between different cosmological simulations in Fig. 12. As before, the exact definitions of recycling vary from study to study, so quantitative differences should not be over-interpreted. For EAGLE, FIRE, and the simulations of Christensen et al. (2016), the median residency time is computed by averaging over all recycling events that occur over the range  $0 < z < 3$ . For Auriga, Grand et al. (2019) defines the residency time slightly differently as the time between launching a wind particle and the time that the particle is either converted into a star, or is re-launched as a wind particle. They compute this residency time as a function of redshift, but since they find it is approximately 500 Myr independent of redshift we simply overplot this value along with the other results. For the NIHAO zoom-in simulations, we take the best-fit relation quoted by Tollet et al. (2019, their equation 11) for the mean residency time of gas that cycles from the ISM to a cool phase in the CGM (and back again), since this is the timescale that they use to compare with the efficiency of recycling in other models and simulations.

Given the variety of definitions employed, Fig. 12 actually shows a surprisingly good consistency between many of the different simulations. Studies that sample a wider dynamic range in halo mass generally find that the median residency time scales negatively with halo mass, ranging from  $\approx 500$  to 750 Myr at  $M_{200} \approx 10^{12} M_{\odot}$ . The two apparent outliers are the results from FIRE and the single simulated halo for which recycling times are presented in Übler et al. (2014). These two studies find significantly shorter recycling times of  $\approx 200$  Myr, and seemingly independent of halo mass in FIRE. We again caution that this could very well reflect differences in the methodologies employed however.

## 4.3 Recycling efficiencies

### 4.3.1 Halo scale

The average residency time (the time between ejection and return) is a poor measure of the efficiency of wind recycling. This is underlined strongly for the specific case of recycling in the EAGLE simulations, since the median residency time for returning gas is  $\approx 0.5$  to 1 Gyr (Fig. 12), but the characteristic return time for all ejected gas to return ranges from 3 to hundreds of Gyr, depending on the halo mass and redshift (Figs. 7 and 13).

As discussed in Section 3.3, we instead measure the efficiency of wind recycling in EAGLE by taking the ratio of the inflow rate of returning gas to the mass of resident ejected gas<sup>4</sup>. This is also the definition of recycling efficiency that is used in most semi-analytic galaxy formation models, and we now consider a comparison between the two. Semi-analytic models generally model recycling explicitly at the halo scale only, with “returning” gas in this case referring to the rate of return of gas back onto the normal “halo-gas” reservoir of circum-galactic gas that resides outside the ISM but still within the halo virial radius. It is usually assumed that the gas ejected beyond the virial radius is powered by stellar feedback, with AGN feedback instead utilised as a mechanism to prevent baryons within the virial radius from reaching the ISM (though see, for example, Bower et al. 2008 for alternative schemes).

<sup>4</sup> Meaning ejected gas that remains outside the ISM for galaxy-scale recycling, or remains outside the virial radius for halo-scale recycling

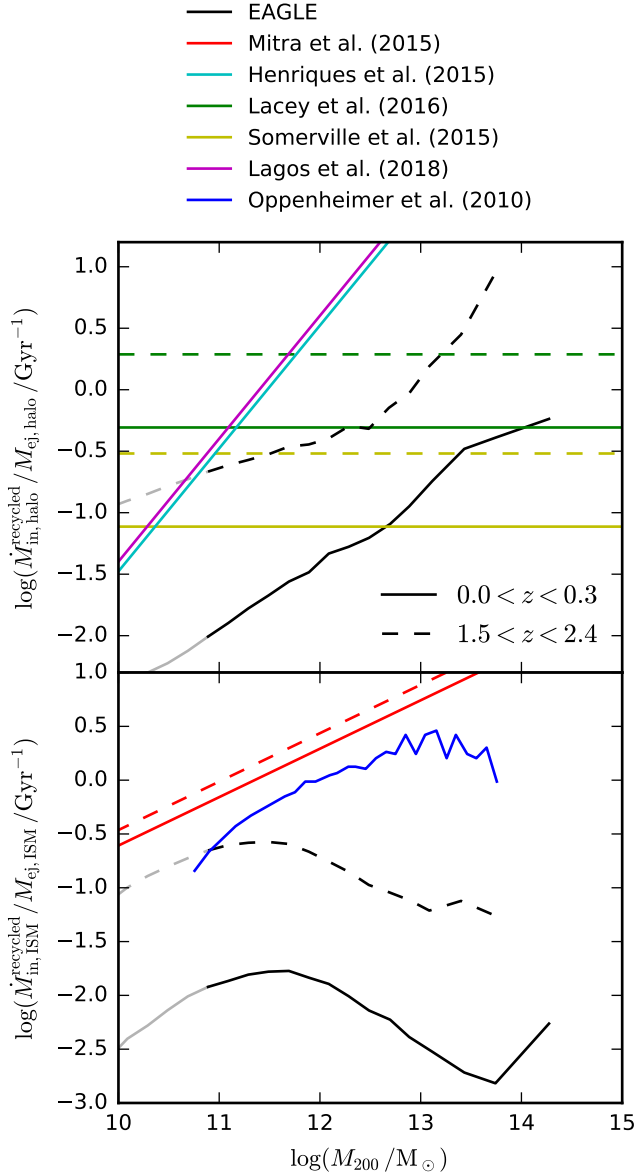


**Figure 13.** The characteristic return efficiency for gas that is ejected from haloes (top panel), and from the ISM of galaxies (bottom panel), as a function of halo mass. We define the efficiency (per Gyr in this case) as  $\dot{M}_{\text{in}}^{\text{recycled}} / M_{\text{ej}}$ , where  $\dot{M}_{\text{in}}^{\text{recycled}}$  is the inflow rate of recycled gas, and  $M_{\text{ej}}$  is the mass of the reservoir of ejected gas. At the halo scale, we compare results from the reference EAGLE simulation (black) with semi-analytic galaxy formation models, including GALFORM (Lacey et al. 2016), L-GALAXIES (Henriques et al. 2015), SHARK (Lagos et al. 2018), and the Santa Cruz model (Somerville et al. 2015). At the galaxy scale, we compare results from EAGLE with the cosmological simulations of Oppenheimer et al. (2010), and the idealised gas regulator model of Mitra et al. (2015). Solid (dashed) lines show results at  $z = 0$  ( $z = 2$ ), with the exception of Oppenheimer et al. (2010), who measure the median time for gas ejected at  $z \approx 1$  to return to the ISM (accounting for non-returning gas), as a function of halo mass at the time of ejection. At the halo scale, the efficiency of gas recycling in EAGLE varies strongly with redshift (fairly consistent with models that assume the efficiency scales with the halo dynamical time), and with a halo mass dependence that is intermediate between the two often considered cases of no dependence, and linear scaling with halo mass. At the galaxy scale, EAGLE finds longer timescales than Oppenheimer et al. (2010) and Mitra et al. (2015), particular at high halo masses where the efficiency drops in EAGLE due (at least in part) to the presence of AGN feedback, which was not included in the simulations of Oppenheimer et al. (2010). Overall, the differences between the different models are very large. © 2018 RAS, MNRAS 000, 1–21

The details then vary slightly from model to model. The GALFORM model (as of Lacey et al. 2016) makes the assumption that the gas ejected from the ISM of galaxies is also ejected beyond the halo virial radius. The Santa Cruz model (as of Somerville et al. 2008 2015) assume that a fraction of the gas ejected from the ISM is immediately reincorporated into the standard halo-gas reservoir, and that a fraction is ejected beyond the halo virial radius (their recycling efficiency then refers to the latter component). The L-Galaxies model of Henriques et al. (2015) and SHARK model of Lagos et al. (2018) make a similar assumption, but also allow for the ejection of halo gas that was not previously part of the ISM. In the L-Galaxies model, the “ejected” gas is conceptually considered to be a combination of gas that is genuinely ejected beyond the virial radius, and of gas that is spatially located within the halo but which is too hot to undergo standard infall from the CGM (this has the disadvantage of leaving the total halo baryon content as a not clearly defined quantity).

Broadly speaking, the definitions of recycling efficiency used in these models are all at least roughly equivalent to our measurements of halo-scale recycling in EAGLE, and we show the comparison between the two in the top panel of Fig. 13. Tellingly, the efficiency of halo-scale recycling can vary by over two orders of magnitude between different models and EAGLE at a given halo mass and redshift, despite the fact that each was calibrated to reproduce the same basic galaxy population diagnostics (such as the galaxy stellar mass function or luminosity function). In Mitchell et al. (2020), a comparison between EAGLE and the same models for galaxy and halo-scale outflows shows differences of comparable order. As discussed in that work, this largely reflects the underlying degeneracy in galaxy formation that the integrated stellar properties of galaxies (that are usually used as constraints for theoretical models and simulations) are only sensitive to the *net* inflow rates of gas onto galaxies, and not to the relative breakdown between first-time inflows, outflows, and wind recycling.

The top panel of Fig. 13 does show some commonality however. The GALFORM and Santa Cruz models assume that the efficiency of halo-scale wind recycling scales inversely with the age of the Universe, which is similar to the evolution in EAGLE at fixed halo mass (as demonstrated explicitly in Fig. 7), albeit the redshift evolution is stronger in EAGLE. Conversely, both the Henriques et al. (2015) L-galaxies model and the (fiducial) SHARK model of Lagos et al. (2018) assume that the recycling efficiency depends linearly and positively with halo mass, which is again similar to EAGLE at fixed redshift, though in this case the halo mass dependence is weaker in EAGLE.

#### 4.3.2 Galaxy scale

The bottom panel of Fig. 13 compares the efficiency of galaxy-scale wind recycling between EAGLE, the cosmological simulation of Oppenheimer et al. (2010), we compare to their preferred “VZW” momentum scaling wind model), and the best-fit “equilibrium” model presented in Mitra et al. (2015). Both Oppenheimer et al. (2010) and Mitra et al. (2015) measure wind recycling at the galaxy scale (i.e. gas that is ejected from and returns to the ISM of galaxies). As with Grand et al. (2019), Oppenheimer et al. (2010) characterise wind recycling by measuring the difference between the time wind particles are launched, and the time wind particles either form a star or are re-launched. Unlike other the analyses presented for other cosmological simulations however, Oppenheimer et al. (2010) include the contribution of non-returning gas particles by setting their residency time to the age of the Universe, and only

quote a median if it is less than this value. While not precisely the same as the definition used for EAGLE (see Section 3.3, which is formally equivalent to the definition used in Mitra et al. 2015), the two quantities are close enough that we believe that the comparison is meaningful. A final caveat however is that Oppenheimer et al. (2010) measure the efficiency of recycling for gas that is ejected at  $z = 1$ , and that returns (or not) over the range  $0 < z < 1$ , as a function of the halo mass at the time of ejection. This does not map straightforwardly onto our measurements in EAGLE (or to Mitra et al. 2015), but we mitigate this by showing our recycling efficiencies at  $z = 2$  and at  $z = 0$ , which should bracket the range used in Oppenheimer et al. (2010).

The bottom panel of Fig. 13 shows that galaxy-scale recycling is apparently more efficient in the simulation of Oppenheimer et al. (2010) than in EAGLE, although our  $z = 2$  results overlap at  $M_{200} \approx 10^{11} M_{\odot}$ . Unlike in EAGLE, where the efficiency of galaxy-scale wind recycling peaks at  $M_{200} \approx 10^{12} M_{\odot}$  (and declines strongly at higher masses), the efficiency of wind recycling continues to rise monotonically with halo mass in the simulation of Oppenheimer et al. (2010). This has the consequence that almost all of the gas accretion onto massive galaxies is recycled in this simulation. Their simulation also significantly over-estimates the abundance of massive galaxies, and both of these properties presumably reflect the lack of any form of AGN feedback in their simulation (although see Huang et al. 2020 for discussion of additional caveats to their stellar feedback model).

The comparison with the best-fit equilibrium model of Mitra et al. (2015) is also worthy of discussion. Mitra et al. (2015) constrain their model against empirically-derived constraints on the relationship between galaxy stellar mass and halo mass, the relationship between galaxy star formation rate and stellar mass, and the relationship between ISM metallicity and stellar mass, all as a function of redshift. Given their adopted parameterisations for preventative feedback, outflows, and recycling, they find a unique solution that fits the data within their parameter space. Furthermore, they report that using only two of the three observational constraints is sufficient to constrain the model. It is therefore interesting to note the greater than order of magnitude difference in recycling efficiency between their best-fit model and EAGLE at  $z = 0$ , especially given that EAGLE was calibrated to produce very similar stellar masses. EAGLE does systematically underpredict galaxy star formation rates for actively star-forming galaxies at a given stellar mass by about 0.3 dex, but otherwise the simulation predicts star formation rates that evolve in time in a way that is broadly consistent with observations (Furlong et al. 2015). In addition, while the reference EAGLE model (at fiducial resolution) does not agree well with the observed galaxy mass-metallicity relationship for  $M_{\star} < 10^{10} M_{\odot}$ , reasonably good agreement is seen for the higher resolution Recal simulation down to  $M_{\star} \sim 10^9 M_{\odot}$  (Schaye et al. 2015). The Recal simulation has qualitatively very similar recycling efficiency to that seen here (see Appendix A1), at least relative to the discrepancy between EAGLE and the model of Mitra et al. (2015).

Putting this together, this reinforces the idea that the stellar properties of galaxies (and possibly even the mass-metallicity relationship) do not strongly constrain the overall network of first-time inflows, outflows and recycling that regulate galaxy evolution. To make progress with simplified analytic and semi-analytic models, we suggest that appropriately defined measurements need to be performed for different hydrodynamical simulations with different implementations of feedback physics, and that the parameterisations adopted in simple models should then be made flexible enough to

match the range in inflow/outflow/recycling efficiencies measured from simulations. With this in place, we suggest that a parameter space search using similar observational constraints to those employed in Mitra et al. (2015) may yield more robust results, albeit with the (likely) conclusion that conventional observational diagnostics of the galaxy population are indeed not sufficiently constraining. The observations that presumably would provide more constraining power, primarily the distribution of ejected metals as a function of distance from the host galaxy, are less readily modelled in simplified analytic or semi-analytic models, but again this could perhaps be mitigated by taking results from different hydrodynamical simulations in the literature to provide a physical prior on which distributions would be reasonable, and to enable a self-consistent link between the assumed mass and energy fluxes of outflows, and the resulting spatial distribution of extra-galactic metals.

#### 4.4 Inflows with super-Lagrangian refinement in the CGM

van de Voort et al. (2019), Peebles et al. (2019), Hummels et al. (2019) and Suresh et al. (2019) have recently explored the effects of using non-Lagrangian criteria to increase the numerical resolution inside the CGM, using cosmological zoom-in simulations. The relative lack of numerical resolution inside the CGM of cosmological simulations has been a longstanding point of discussion, and the afore-mentioned studies show that tracers of dense gas in the CGM do change when resolution of low-density CGM phases is increased.

The impact of this on inflowing gas fluxes onto galaxies is currently unclear, although presumably fairly minor since the properties of the host galaxy are not reported to change significantly when the CGM resolution is changed (Peebles et al. 2019). The detailed trajectories and relative importance of different gas accretion channels could still be affected however. If thermal instabilities do lead to significant conversion of mass from a hot thermal wind into cold dense clumps, this would presumably have a significant impact on subsequent gas recycling. The relatively dense phases of gas that are stripped from satellites could also be conceivably affected, perhaps altering the importance of the transfer and merger components discussed in this work. These questions look set to inspire continued work using zoom-in simulations in the coming years.

## 5 SUMMARY

We have measured gaseous inflow rates onto galaxies and their associated dark matter haloes in the EAGLE simulations. By tracking particles after they are ejected from galaxies and/or haloes, we quantify the relative importance and efficiencies of first time gaseous-infall, wind recycling, and the transfer of ejected gas between independent galaxies and haloes. For wind recycling, we select only gas that first outflows with a time-integrated radial velocity greater than one quarter of the halo maximum circular velocity, over at least one quarter of a halo dynamical time, corresponding to a radial displacement of  $\approx 15$  kpc for a Milky Way-mass halo at low redshift. Our measurements focus therefore on recycling of gas that has moved outwards over spatial and temporal scales that are significant relative to the associated scales of the dark matter halo, and do not account for any galactic fountains that occur on smaller scales at the disk-halo interface.

Qualitatively consistent with earlier results from the Overwhelmingly Large Simulations project (OWLS, van de Voort et al. 2011), we find that for gas accretion onto the ISM of galaxies,



inflow rates per unit halo mass clearly peak for a halo mass of  $\sim 10^{12} M_{\odot}$  (Fig. 1), which helps to explain the empirically inferred relationship between galaxy stellar mass and halo mass (e.g. Behroozi et al. 2010; Moster et al. 2010), and therefore the shape of the observed galaxy stellar mass function.

Gaseous accretion rates onto haloes are reduced relative to (scaled) dark matter accretion rates for haloes with  $M_{200} < 10^{13} M_{\odot}$ . As demonstrated in Wright et al. (2020), the reduction of gas accretion (relative to dark matter accretion) at the virial radius is connected primarily to the implementation of feedback processes in EAGLE, which is demonstrated by comparing halo-scale accretion rates of first-time and recycled infall between the fiducial EAGLE simulations and simulation variations with feedback and/or radiative cooling processes removed. Here, we show that instantaneous first-time gaseous infall is slightly suppressed relative to first-time infalling dark matter for  $M_{200} < 10^{11} M_{\odot}$ , but actually exceeds dark matter accretion at higher halo masses (Fig. 3). Considering instead the time-integrated mass of first-time infall at the virial radius (Fig. 4), we show that the integrated gas accretion onto haloes is slightly suppressed for  $M_{200} < 10^{12} M_{\odot}$  (by up to 0.4 dex), and is slightly enhanced at higher halo masses (by up to 0.2 dex). At the transition mass of  $M_{200} = 10^{12} M_{\odot}$ , we show in Fig. 5 that first-time gas accretion at the virial radius is not “prevented” at the virial radius by  $z = 0$ , but is rather delayed from the peak epoch of specific halo growth (at  $z \approx 4$ ), to slightly later times ( $z \approx 3$ ). This effect may partly explain why observed galaxy growth does not appear to closely trace the time evolution of predicted halo mass growth (Daddi et al. 2007; Dekel & Mandelker 2014; Mitchell et al. 2014).

Splitting gas accretion onto galaxies and haloes between first-time infall, recycled accretion, transfer between independent galaxies/haloes, and mergers, we find that first-time infall usually provides the largest single contribution (Fig. 2). This differs from some other simulations with different implementations of stellar feedback (Anglés-Alcázar et al. 2017; Grand et al. 2019), who find significantly higher contributions from recycled or transferred gas (Fig. 11). The results from EAGLE follow from our study of outflows, presented in Mitchell et al. (2020), where we show that, relative to other simulations, outflows in EAGLE are driven out over larger scales, and with mass fluxes that increase with radius, such that more gas is being ejected from haloes than from the ISM of galaxies. In this picture, the natural expectation is that recycling is less efficient as a mechanism to bring gas back to galaxies. We note that at least for low-mass haloes, outflows must reach far beyond the halo virial radius to account for the high rate of incidence of weak metal lines in blind quasar absorption surveys (e.g. Booth et al. 2012).

We measure the efficiency of first-time infall from the CGM onto the ISM (Fig. 6), defined as the ratio between cosmic time and the characteristic timescale for the CGM to accrete onto the galaxy. This efficiency is insensitive to halo mass for  $M_{200} < 10^{12} M_{\odot}$ , and drops sharply at higher halo masses. This is qualitatively consistent with the traditional picture for galaxy formation, in which gas infall within low-mass haloes is limited by gravitational timescales (which are scale free), and by radiative cooling timescales (which are increased by AGN feedback) in higher-mass haloes (see also Correa et al. 2018a; Davies et al. 2020). At fixed halo mass, infall efficiencies decrease with time, which for  $M_{200} < 10^{12} M_{\odot}$  implies that there is more than just a basic dependence on the radial gravitational freefall time.

We also measure the efficiency of wind recycling at both galaxy (recycling of gas leaving/rejoining the ISM) and halo (re-

cycling of gas at the virial radius) scales (Fig. 7), with the efficiency defined as the ratio between cosmic time and the characteristic timescale for ejected gas to return, accounting for gas that never returns. The efficiency of halo-scale wind recycling evolves at fixed mass, decreasing at lower redshifts. The efficiency of halo-scale wind recycling increases with halo mass, but with a power law exponent ( $\approx 0.6$ ) that is smaller than the value of unity adopted by several recent semi-analytic galaxy formation models (Henriques et al. 2013; Hirschmann et al. 2016; Lagos et al. 2018).

Wind recycling onto the ISM of galaxies is generally less efficient than wind recycling onto haloes (Fig. 7), and (when considering all of the gas ejected from galaxies) clearly peaks at a characteristic halo mass of  $M_{200} \sim 10^{12} M_{\odot}$ , reflecting the peak in total galaxy accretion rates at this mass. Wind recycling therefore plays an active role in shaping the characteristic Schechter-function-like shape of the galaxy stellar mass function in EAGLE. If we consider the efficiency of wind recycling for only the subset of gas that has not escaped the halo (Fig. 8), we find that the efficiency of CGM-scale wind recycling is actually higher than the efficiency of first-time infall from the CGM, and declines strongly with increasing halo mass.

At  $z = 0$ , most of the gas ejected from galaxies resides between 2 and 4 times the halo virial radius (Fig. 10). Gas that returns to galaxies generally has not left the halo however, with half of the returning gas at  $z = 0$  having reached only a quarter of the halo virial radius before falling back.

By comparing the efficiency of wind recycling between EAGLE and semi-analytic models, we show differences between models and EAGLE that span orders of magnitude at fixed halo mass and redshift (Fig. 13), highly reminiscent of a similar comparison of outflow rates presented in Mitchell et al. (2020). This strongly emphasises the point that the “baryon cycle” (meaning the overall network of inflows, outflows and recycling) is deeply degenerate, with conventional extra-galactic observational constraints only constraining the *net* inflow of gas onto galaxies.

With this degeneracy in mind, it would be very timely to review if cosmological simulations (each with different implementations of uncertain star formation and feedback processes) yield similarly discrepant recycling efficiencies. Unfortunately, the majority of analyses of wind recycling in state-of-the-art cosmological simulations have not presented measurements of the efficiency of wind recycling in a way that accounts for non-returning gas (which is an essential component in the EAGLE simulations), and we strongly encourage future analyses of other simulations to present such measurements.

## ACKNOWLEDGEMENTS

We would like to thank Dr. John Helly for producing and sharing the halo merger trees that form the backbone of our analysis. We thank Claudia Lagos and Ruby Wright for useful discussions.

This work used the DiRAC@Durham facility managed by the Institute for Computational Cosmology on behalf of the STFC DiRAC HPC Facility (www.dirac.ac.uk). The equipment was funded by BEIS capital funding via STFC capital grants ST/K00042X/1, ST/P002293/1, ST/R002371/1 and ST/S002502/1, Durham University and STFC operations grant ST/R000832/1. DiRAC is part of the National e-Infrastructure.

This work was supported by Vici grant 639.043.409 from the Netherlands Organisation for Scientific Research (NWO).

RGB acknowledges support from the Durham consolidated grant: ST/P000541/1.

## DATA AVAILABILITY

The data underlying this article will be shared on reasonable request to the corresponding author. Raw particle data and merger trees for the EAGLE simulations have been publicly released (McAlpine et al. 2016).

## REFERENCES

- Anglés-Alcázar D., Faucher-Giguère C.-A., Kereš D., Hopkins P. F., Quataert E., Murray N., 2017, *MNRAS*, 470, 4698
- Bahé Y. M., McCarthy I. G., Balogh M. L., Font A. S., 2013, *MNRAS*, 430, 3017
- Behroozi P. S., Conroy C., Wechsler R. H., 2010, *ApJ*, 717, 379
- Bish H. V., Werk J. K., Prochaska J. X., Rubin K. H. R., Zheng Y., O’Meara J. M., Deason A. J., 2019, *ApJ*, 882, 76
- Booth C. M., Schaye J., 2009, *MNRAS*, 398, 53
- Booth C. M., Schaye J., Delgado J. D., Dalla Vecchia C., 2012, *MNRAS*, 420, 1053
- Borrow J., Anglés-Alcázar D., Davé R., 2020, *MNRAS*, 491, 6102
- Bower R. G., Benson A. J., Malbon R., Helly J. C., Frenk C. S., Baugh C. M., Cole S., Lacey C. G., 2006, *MNRAS*, 370, 645
- Bower R. G., McCarthy I. G., Benson A. J., 2008, *MNRAS*, 390, 1399
- Bower R. G., Schaye J., Frenk C. S., Theuns T., Schaller M., Crain R. A., McAlpine S., 2017, *MNRAS*, 465, 32
- Christensen C. R., Davé R., Governato F., Pontzen A., Brooks A., Munshi F., Quinn T., Wadsley J., 2016, *ApJ*, 824, 57
- Collacchioni F., Lagos C. D. P., Mitchell P. D., Schaye J., Wisnioski E., Cora S. A., Correa C. A., 2019, *arXiv e-prints*, arXiv:1910.05377
- Correa C. A., Schaye J., van de Voort F., Duffy A. R., Wyithe J. S. B., 2018a, *MNRAS*, 478, 255
- Correa C. A., Schaye J., Wyithe J. S. B., Duffy A. R., Theuns T., Crain R. A., Bower R. G., 2018b, *MNRAS*, 473, 538
- Correa C. A., Wyithe J. S. B., Schaye J., Duffy A. R., 2015, *MNRAS*, 450, 1521
- Crain R. A. et al., 2015, *MNRAS*, 450, 1937
- Croton D. J. et al., 2006, *MNRAS*, 365, 11
- Daddi E. et al., 2007, *ApJ*, 670, 156
- Dalla Vecchia C., Schaye J., 2012, *MNRAS*, 426, 140
- Davé R., Finlator K., Oppenheimer B. D., 2012, *MNRAS*, 421, 98
- Davies J. J., Crain R. A., Oppenheimer B. D., Schaye J., 2020, *MNRAS*, 491, 4462
- Dekel A., Birnboim Y., 2006, *MNRAS*, 368, 2
- Dekel A., Mandelker N., 2014, *MNRAS*, 444, 2071
- Dolag K., Borgani S., Murante G., Springel V., 2009, *MNRAS*, 399, 497
- Faucher-Giguère C.-A., Kereš D., Ma C.-P., 2011, *MNRAS*, 417, 2982
- Fox A. J. et al., 2014, *ApJ*, 787, 147
- Fraternali F., 2017, *Astrophysics and Space Science Library*, Vol. 430, *Gas Accretion via Condensation and Fountains*, Fox A., Davé R., eds., p. 323
- Furlong M. et al., 2015, *MNRAS*, 450, 4486
- Genel S., Bouché N., Naab T., Sternberg A., Genzel R., 2010, *ApJ*, 719, 229
- Grand R. J. J. et al., 2017, *MNRAS*, 467, 179
- Grand R. J. J. et al., 2019, *MNRAS*, 490, 4786
- Hafen Z. et al., 2019, *MNRAS*, 488, 1248
- Henriques B. M. B., White S. D. M., Thomas P. A., Angulo R., Guo Q., Lemson G., Springel V., Overzier R., 2015, *MNRAS*, 451, 2663
- Henriques B. M. B., White S. D. M., Thomas P. A., Angulo R. E., Guo Q., Lemson G., Springel V., 2013, *MNRAS*, 431, 3373
- Hirschmann M., De Lucia G., Fontanot F., 2016, *MNRAS*, 461, 1760
- Hopkins P. F., Kereš D., Oñorbe J., Faucher-Giguère C.-A., Quataert E., Murray N., Bullock J. S., 2014, *MNRAS*, 445, 581
- Huang S., Katz N., Davé R., Oppenheimer B. D., Weinberg D. H., Fardal M., Kollmeier J. A., Peebles M. S., 2020, *MNRAS*, 493, 1
- Hummels C. B. et al., 2019, *ApJ*, 882, 156
- Jiang L., Helly J. C., Cole S., Frenk C. S., 2014, *MNRAS*, 440, 2115
- Katz N., Keres D., Dave R., Weinberg D. H., 2003, *Astrophysics and Space Science Library*, Vol. 281, *How Do Galaxies Get Their Gas?*, Rosenberg J. L., Putman M. E., eds., p. 185
- Kaviraj S. et al., 2017, *MNRAS*, 467, 4739
- Kennicutt, Jr. R. C., 1998, *ApJ*, 498, 541
- Kereš D., Katz N., Weinberg D. H., Davé R., 2005, *MNRAS*, 363, 2
- Lacey C. G. et al., 2016, *MNRAS*, 462, 3854
- Lagos C. d. P., Tobar R. J., Robotham A. S. G., Obreschkow D., Mitchell P. D., Power C., Elahi P. J., 2018, *MNRAS*, 481, 3573
- Larson R. B., 1972, *Nature Physical Science*, 236, 7
- Madau P., Dickinson M., 2014, *ARA&A*, 52, 415
- Marasco A., Crain R. A., Schaye J., Bahé Y. M., van der Hulst T., Theuns T., Bower R. G., 2016, *MNRAS*, 461, 2630
- McAlpine S. et al., 2016, *Astronomy and Computing*, 15, 72
- Mitchell P. D., Blaizot J., Devriendt J., Kimm T., Michel-Dansac L., Rosdahl J., Slyz A., 2018, *MNRAS*, 474, 4279
- Mitchell P. D., Lacey C. G., Cole S., Baugh C. M., 2014, *MNRAS*, 444, 2637
- Mitchell P. D., Schaye J., Bower R. G., Crain R. A., 2020, *MNRAS*, 494, 3971
- Mitra S., Davé R., Finlator K., 2015, *MNRAS*, 452, 1184
- Moster B. P., Somerville R. S., Maulbetsch C., van den Bosch F. C., Macciò A. V., Naab T., Oser L., 2010, *ApJ*, 710, 903
- Muratov A. L., Kereš D., Faucher-Giguère C.-A., Hopkins P. F., Quataert E., Murray N., 2015, *MNRAS*, 454, 2691
- Neistein E., Khochfar S., Dalla Vecchia C., Schaye J., 2012, *MNRAS*, 421, 3579
- Nelson D., Genel S., Vogelsberger M., Springel V., Sijacki D., Torrey P., Hernquist L., 2015, *MNRAS*, 448, 59
- Nelson D. et al., 2019, *MNRAS*, 490, 3234
- Nelson D., Vogelsberger M., Genel S., Sijacki D., Kereš D., Springel V., Hernquist L., 2013, *MNRAS*, 429, 3353
- Oppenheimer B. D., Davé R., Kereš D., Fardal M., Katz N., Kollmeier J. A., Weinberg D. H., 2010, *MNRAS*, 406, 2325
- Peebles M. S. et al., 2019, *ApJ*, 873, 129
- Pillepich A. et al., 2018, *MNRAS*, 473, 4077
- Planck Collaboration et al., 2014, *A&A*, 571, A16
- Rees M. J., Ostriker J. P., 1977, *MNRAS*, 179, 541
- Roberts-Borsani G. W., Saintonge A., 2019, *MNRAS*, 482, 4111
- Romano-Díaz E., Garaldi E., Borzyszkowski M., Porciani C., 2017, *MNRAS*, 469, 1809

Rosas-Guevara Y. M. et al., 2015, MNRAS, 454, 1038  
 Rubin K. H. R., Prochaska J. X., Koo D. C., Phillips A. C., 2012, ApJ, 747, L26  
 Schaye J., 2004, ApJ, 609, 667  
 Schaye J. et al., 2015, MNRAS, 446, 521  
 Schaye J., Dalla Vecchia C., 2008, MNRAS, 383, 1210  
 Scoville N. et al., 2017, ApJ, 837, 150  
 Somerville R. S., Hopkins P. F., Cox T. J., Robertson B. E., Hernquist L., 2008, MNRAS, 391, 481  
 Somerville R. S., Popping G., Trager S. C., 2015, MNRAS, 453, 4337  
 Springel V., 2005, MNRAS, 364, 1105  
 Springel V. et al., 2005, Nature, 435, 629  
 Springel V., White S. D. M., Tormen G., Kauffmann G., 2001, MNRAS, 328, 726  
 Stevens A. R. H., del P. Lagos C., Contreras S., Croton D. J., Padilla N. D., Schaller M., Schaye J., Theuns T., 2017, MNRAS  
 Suresh J., Nelson D., Genel S., Rubin K. H. R., Hernquist L., 2019, MNRAS, 483, 4040  
 Tollet É., Cattaneo A., Macciò A. V., Dutton A. A., Kang X., 2019, MNRAS, 485, 2511  
 Turner M. L., Schaye J., Crain R. A., Rudie G., Steidel C. C., Strom A., Theuns T., 2017, MNRAS, 471, 690  
 Übler H., Naab T., Oser L., Aumer M., Sales L. V., White S. D. M., 2014, MNRAS, 443, 2092  
 van Daalen M. P., Schaye J., 2015, MNRAS, 452, 2247  
 van de Voort F., 2017, Astrophysics and Space Science Library, Vol. 430, The Effect of Galactic Feedback on Gas Accretion and Wind Recycling, Fox A., Davé R., eds., p. 301  
 van de Voort F., Bahé Y. M., Bower R. G., Correa C. A., Crain R. A., Schaye J., Theuns T., 2017, MNRAS, 466, 3460  
 van de Voort F., Schaye J., Booth C. M., Haas M. R., Dalla Vecchia C., 2011, MNRAS, 414, 2458  
 van de Voort F., Springel V., Mandelker N., van den Bosch F. C., Pakmor R., 2019, MNRAS, 482, L85  
 Vogelsberger M. et al., 2014, MNRAS, 444, 1518  
 Wiersma R. P. C., Schaye J., Smith B. D., 2009, MNRAS, 393, 99  
 Wright R. J., Lagos C. d. P., Power C., Mitchell P. D., 2020, arXiv e-prints, arXiv:2006.00924  
 Zabl J. et al., 2019, MNRAS, 485, 1961

## APPENDIX A: CONVERGENCE

### A1 Resolution convergence

Fig. A1 compares gas accretion rates between the Reference EAGLE (at fiducial EAGLE resolution) and Recal EAGLE models (at eight times higher mass resolution). We use a common  $(25 \text{ Mpc})^3$  volume for both models. The left panels of Fig. A1 show that inflow rates are reasonably converged between the two resolutions in higher-mass haloes,  $M_{200} > 10^{12} M_{\odot}$  at  $z \approx 0$  and  $M_{200} > 10^{11} M_{\odot}$  at  $z \approx 3$ , but are not well converged at lower halo masses, especially at the galaxy scale (bottom-left panel) for which inflow rates can be up to  $\approx 0.5$  dex higher in the Recal model (for  $M_{200} = 10^{11} M_{\odot}$  at  $z = 0$ ). The higher inflow rates seen in the Recal model also apply to each of the separated contributions from first-time, recycled, and transferred accretion (right panels). The exception is transferred accretion at the halo scale, which is well converged between the two simulations.

Qualitatively, our results remain similar between the Reference and Recal models. The most clear and important quantitative

difference is the characteristic halo mass for which galaxy-scale inflow rates peak, which is lower (and the peak broader) in the Recal model, at  $M_{200} \approx 10^{11} M_{\odot}$ . We intend to explore the implications of this difference for the relationship between galaxy stellar mass and halo mass in future work (the stellar mass to halo mass ratio does still peak at  $M_{200} \approx 10^{12} M_{\odot}$  in the Recal model, Schaye et al. 2015).

### A2 Temporal convergence

We use 200 discrete simulation outputs (referred to as snapshots) to track the movements of particles in post-processing from our simulations. The time sampling of these snapshots is shown in appendix A1 of Mitchell et al. (2020). This sampling affects our results in the sense that insufficient time resolution will cause us to miss inflowing particles that are then ejected within a timescale that is smaller than the separation between snapshots. In Mitchell et al. (2020), we showed that outflow rates are fairly well (but not fully) converged for our fiducial snapshot grid.

Fig. A2 shows the corresponding picture for total inflow rates onto haloes (top) and galaxies (bottom), using a  $(25 \text{ Mpc})^3$  volume for which five times more snapshots are available. As with outflows, we find that galaxy-scale inflow rates converge fairly well for  $M_{200} < 10^{12} M_{\odot}$ , but convergence is less good at higher-halo masses, particularly at low redshift. Inflow rates are less well converged at the halo scale for low-mass galaxies, and increase by roughly 50% after increasing the number of snapshots by a factor 5 relative to our fiducial spacing. If we instead consider the fractional contribution of different accretion channels to the total inflow rate (not shown), the fractional contributions are well converged at our fiducial snapshot cadence at the halo scale, and for  $M_{200} \geq 10^{12} M_{\odot}$  at the galaxy scale. At the galaxy scale, the fractional contribution of (for example) recycled gas increases by  $\approx 30\%$  at  $z \sim 0$  if we increase the snapshot cadence by a factor five for  $M_{200} \sim 10^{11} M_{\odot}$ .

Quantitatively our results are therefore affected by the available snapshot cadence, although qualitatively our results are unaffected (consistent with conclusions of a similar check by van de Voort et al. 2017). This guides our choice to use as many simulation snapshots as possible, which is 200 for the flagship simulation.

## APPENDIX B: METHODOLOGY DETAILS

### B1 Varying the definition of recycling versus transferred accretion

In our fiducial analysis we consider “recycled” gas accretion as being gas that was previously in the ISM (for our galaxy-scale measurements) of any progenitor of the current galaxy. “Transferred” gas accretion is correspondingly considered as gas that was previously in the ISM of any non-progenitor galaxy (this can include gas that was ejected from surviving satellites of the current central galaxy). This differs from other studies in the literature, which have defined “recycled” accretion as gas originating only from the main progenitor of the current galaxy, with “transferred” gas in this case also including gas that was ejected from other progenitors that have since merged with the central galaxy.

Fig. B1 shows the effect of changing from our fiducial definition to the latter alternative definition (which we label here as “MP-only”). The effects of changing the definition are minor for the recycled gas accretion rates, at both halo and galaxy scales. The

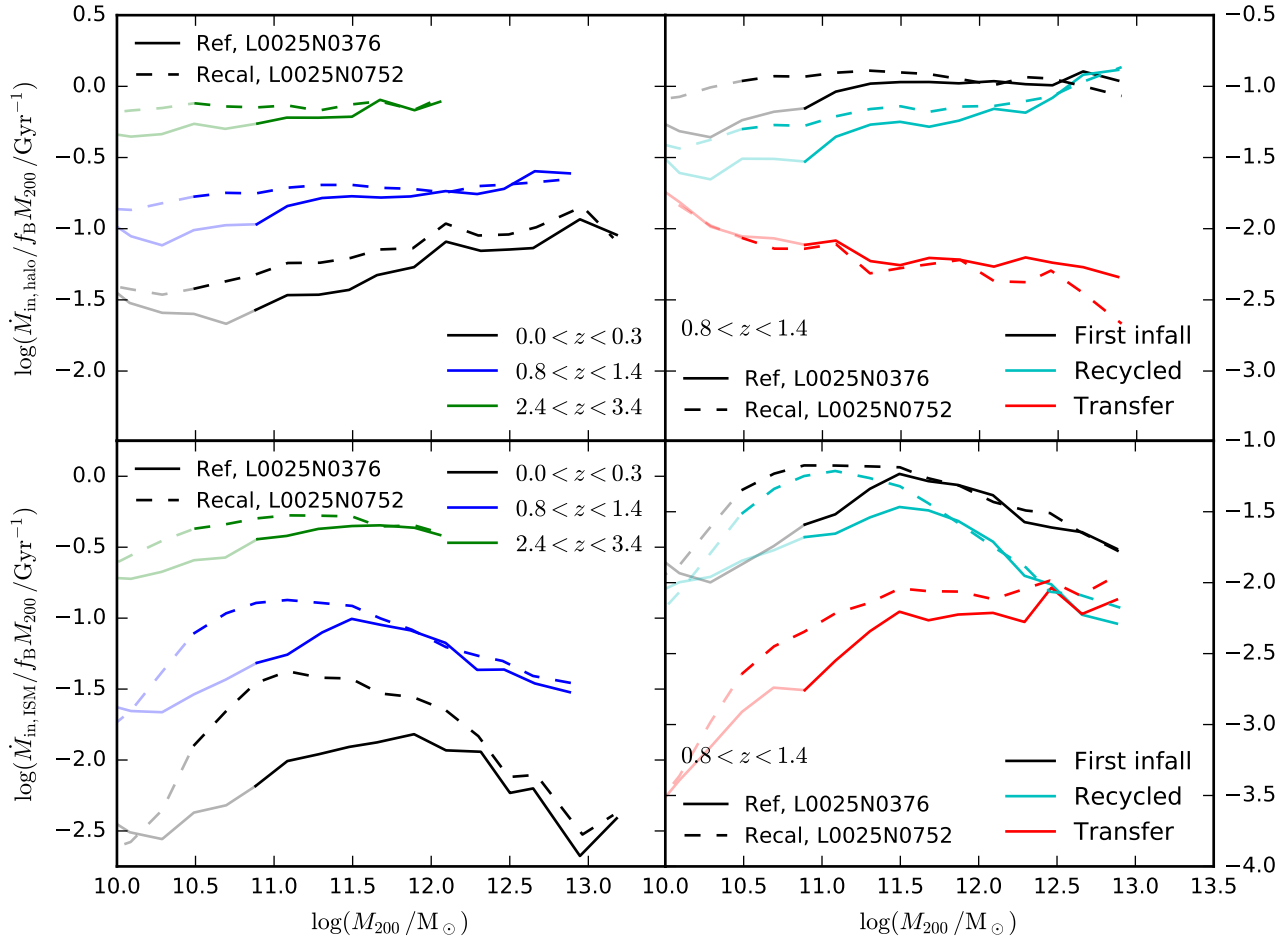


**Figure A1.** A comparison of gaseous inflow rates between a standard-resolution EAGLE simulation of a  $(25 \text{ Mpc})^3$  volume with reference-model parameters (Ref, L0025N0376, where the naming convention is L + box length + N + cube root of the number of particles), and a recalibrated higher-resolution (eight times higher mass resolution) re-simulation of the same volume (Recal, L0025N0752). Top (bottom) panels show inflow rates onto haloes (galaxies). The left (right) panels show the total smooth inflow rate for three redshift ranges, as labelled. The right panels show the separate contributions from first-infalling gas, recycled gas, and transferred gas, over the interval  $0.8 < z < 1.4$ . Transparent lines indicate the range where there are fewer than 100 stellar particles per galaxy. Inflow rates are reasonably well converged for  $M_{200} > 10^{11.5} M_{\odot}$ , but are higher in the higher-resolution Recal simulation for  $M_{200} < 10^{11.5} M_{\odot}$ , most notably on galaxy scales at  $M_{200} \approx 10^{11} M_{\odot}$  at  $z \approx 0$ . This also applies to each of the individual inflow channels (right panels), with the exception of halo gas transfer.

fractional impact is larger for the transferred gas accretion rates, which are modestly increased using the alternative definition.

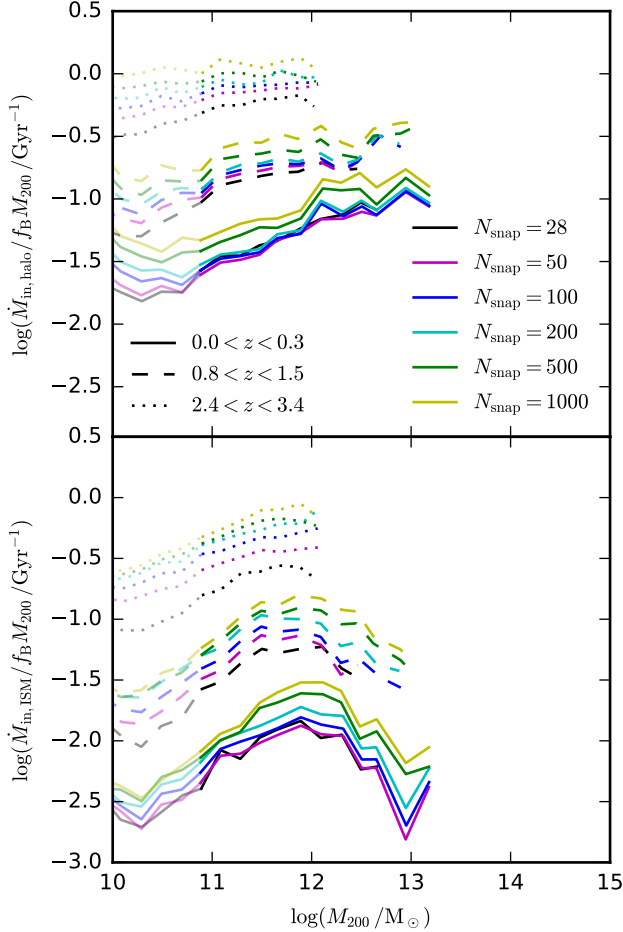
## B2 Varying the velocity cut used to define recycled accretion

As discussed in detail in Mitchell et al. (2020), we use a time-integrated radial velocity cut (averaged over one quarter of a halo dynamical time) to define which particles have been ejected from the ISM (or halo). This affects the amount of recycled gas accretion, with a higher velocity cut resulting in lower recycled gas accretion rates. Fig. B2 shows the impact of varying this cut up and down by a factor two from our fiducial cut (which is at  $0.25 V_{\text{max}}$ , where  $V_{\text{max}}$  is the maximum halo circular velocity). The impact is negligible at the halo scale, but makes a modest difference to recycling rates at the galaxy scale (at the level of tens of percent).

## B3 Varying the halo mass cut used to define first-time, recycled, and transferred accretion

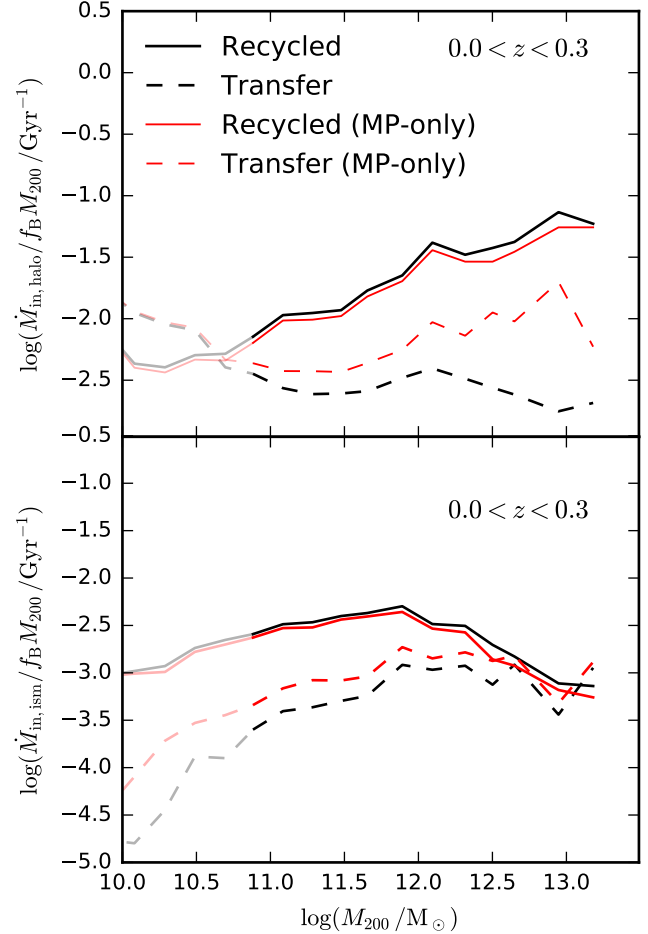
At the galaxy scale, we consider “smooth” accretion (as opposed to “lumpy” accretion via galaxy mergers) to be gas that is accreted while not within the ISM of a subhalo with mass above a given threshold, which we set at  $9.7 \times 10^8 M_{\odot}$ , corresponding to the mass of 100 dark matter particles at the fiducial EAGLE resolution. For smooth accretion, we only consider accreted gas as being recycled or transferred if it was previously within the ISM of a subhalo with mass above the same threshold. We use the same definitions at the halo scale, though in this case we base the different accretion modes on whether gas was previously within the virial radius of a halo with mass above the threshold, without needing to have been within the ISM in the past.

Fig. B3 shows the effect of changing this halo mass threshold up and down by a factor ten. Generally speaking, accretion rates have converged at our fiducial mass cut (but would change if we used a higher mass cut, dotted lines). This implies that the compar-



**Figure A2.** The dependence of inflow rates on the snapshot cadence. Top (bottom) panels show total gaseous accretion rates onto haloes (onto galaxies), plotted as a function of halo mass. Different lines correspond to different numbers of simulation snapshots used to perform the analysis, with 200 being the reference number used in this study (see appendix A1 in Mitchell et al. 2020 for the precise time spacing). Here, we use a smaller (25 Mpc)<sup>3</sup> volume simulation, for which a higher snapshot cadence is available. Transparent lines indicate the range where there are fewer than 100 stellar particles per galaxy. Temporal convergence is reasonably good at the ISM scale (but not excellent at higher masses at lower redshifts). Convergence is less convincing at the halo scale, but only affects the normalisation of our results, at the level of tens of percent.

ison between EAGLE and cosmological zoom-in simulations presented in Section 4.1 is unaffected by our comparative inability to resolve lower-mass haloes in EAGLE (due to the lower numerical resolution employed). The exception in terms of convergence is for “transferred” gas at the halo scale (cyan line, top panel), for which the rates increase by roughly a factor two if we lower the mass threshold by a factor ten. Halo-scale gas transfer aside, we interpret the convergence of our results at a threshold of  $9.7 \times 10^8 M_\odot$  as likely being related to the halo mass scale below which galaxies are prevented from efficiently forming due to photo-heating from the UVB.



**Figure B1.** The impact of changing the definition of recycled accretion from the fiducial definition (solid lines), where gas is considered recycled if it was ejected from any progenitor of the current subhalo, to an alternative definition (*MP-only*, dashed lines) for which only gas ejected from the main progenitor subhalo is considered as recycled, with gas ejected from other progenitors instead labelled as *transfer*. Plotted are the average rates of recycled and transferred accretion for gas being both ejected from, and then later accreting onto, haloes (top panel), and the ISM of galaxies (bottom panel), as a function of halo mass. Transparent lines indicate the range where there are fewer than 100 stellar particles per galaxy. Results are plotted for redshifts  $0 < z < 0.3$ , but the conclusions are very similar at other redshifts. Changing the recycling definition to only gas ejected from the main progenitor makes little difference to our results for recycling, but increases the contribution of halo-scale gas transfer at high halo masses.

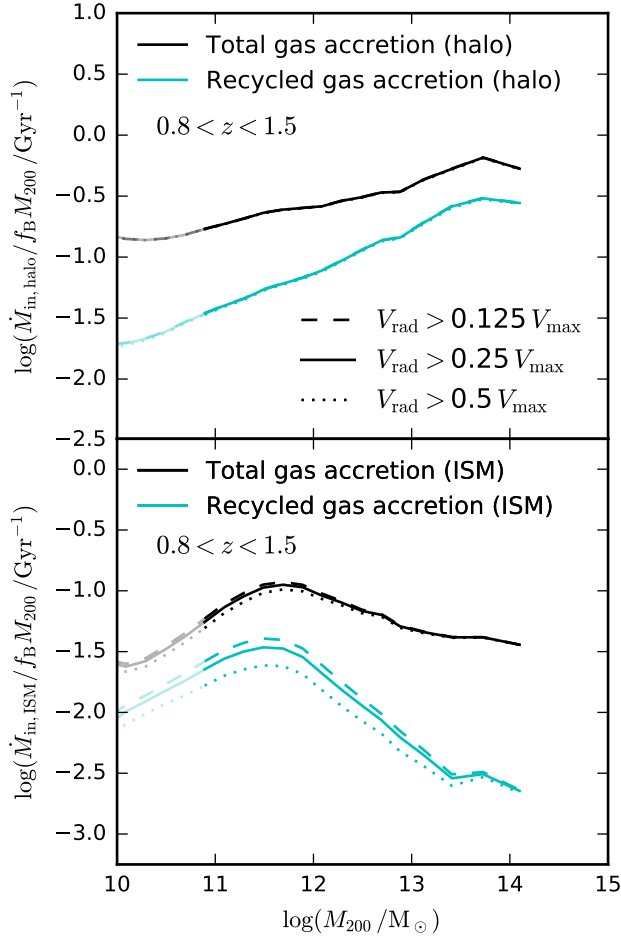


**Figure B2.** The impact of changing the (time-integrated) radial velocity cut used to select outflowing gas that is being ejected from haloes (top panel) and from the ISM of galaxies (bottom panel). Gas accretion rates are plotted at  $z \sim 1$  as a function of halo mass; results are very similar at other redshifts. Black (cyan) lines show total (recycled) gas accretion rates. Transparent lines indicate the range where there are fewer than 100 stellar particles per galaxy. Changing the velocity cut by a factor two makes virtually no difference at the halo scale, or for total accretion rates at the galaxy scale, but has a minor effect on recycled gas accretion rates at the galaxy scale.

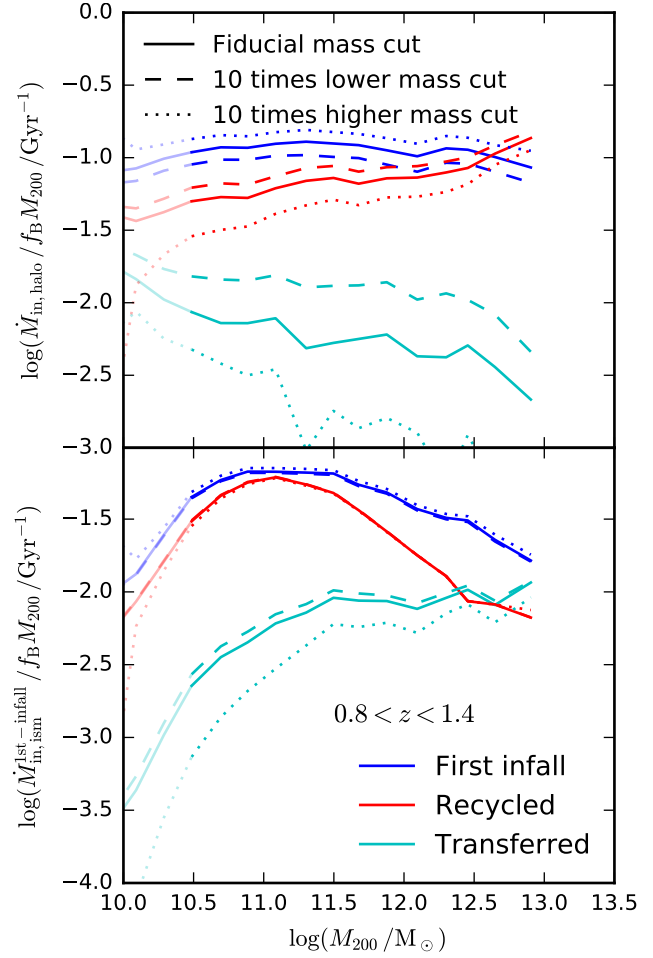


**Figure B3.** The impact of changing the halo mass cuts used to define smooth accretion versus accretion of satellites, and to define the selection of first-time (blue), recycled (red), and transferred (cyan) gaseous accretion (see main text for details). The fiducial halo mass cut (solid lines) is made at  $9.7 \times 10^8 M_\odot$ , corresponding to 100 dark matter particles at standard EAGLE resolution. Here, we use the higher resolution Recal simulation to enable a meaningful exploration of changing our fiducial mass cut to both ten times lower (dashed) and ten times higher values (dotted). The top panel shows inflow rates onto haloes, and the bottom panel shows inflow rates onto the ISM of central galaxies. Results are plotted for  $z \sim 1$ , but are very similar at other redshifts. Transparent lines indicate the range where there are fewer than 100 stellar particles per galaxy. Inflow rates are generally well converged at our fiducial mass cut (relative to the lower mass cut), but adopting a ten times higher mass cut would result in less recycling and transferred accretion. The exception is for gas being transferred onto the halo (bottom-right panel), for which our fiducial mass cut is not converged compared to the lower mass cut, implying that we underestimate the fraction of transferred accretion onto haloes in our fiducial analysis.